lubricants

MDPI

Article

Microstructure, Mechanical Strength, and Tribological Behavior of B_4C/WS_2-Hybrid-Reinforced B319 Aluminum Matrix Composites

Ufuk Tasci

Department of Technical Sciences Vocational School, Gazi University, 06374 Ankara, Turkey; ufuktasci@gazi.edu.tr

Abstract: Hybrid B319 aluminum matrix composites reinforced with 10 wt% B_4C and varying WS_2 contents were fabricated to improve mechanical and tribological performance. The composite containing 2 wt% WS_2 showed the best overall results, with a 29% increase in microhardness (104.3 HV) and a 20% improvement in transverse rupture strength (196.3 MPa) compared to unreinforced B319. Additionally, the friction coefficient dropped by 64% (from 0.497 to 0.178), and the specific wear rate was reduced to 4.34×10^{-6} $mm^3/N{\cdot}m$. Microstructural analyses confirmed homogeneous reinforcement distribution and adequate interfacial bonding. These enhancements are attributed to the dual action of B4C-induced strengthening and WS_2-mediated tribo-film formation, offering a promising solution for lightweight, wear-resistant components in engineering applications.

Keywords: B319 alloy; hybrid composite; B_4C; WS_2; mechanical properties; tribology behaviour

1. Introduction

In recent years, the urgent demand for environmentally friendly and fuel-efficient transportation systems has stimulated the development of lightweight structural materials, particularly in aerospace and electric/hybrid vehicle industries [1,2]. Among lightweight metals, aluminum (Al) and its alloys are widely preferred due to their high strength-to-weight ratio, corrosion resistance, and good castability. Notably, B319 aluminum alloy (Al-Si–Cu) is extensively used in automotive components such as cylinder heads, transmission parts, and engine blocks due to its excellent thermal and mechanical properties, as reported by Kumar and Bichler [3], who investigated the influence of TiC additions on the mechanical behavior of B319 alloy and observed notable improvements in grain refinement and strength. However, previous studies have highlighted that B319 suffers from several limitations when subjected to demanding service environments. In particular, its vulnerability to thermal fatigue, reduced dimensional stability at elevated temperatures, and rapid wear under high-load or dry sliding conditions restrict its broader application in performance-critical components [4]. These challenges underscore the need for a dual-function reinforcement approach aimed at enhancing both structural strength and wear durability. Several strategies have been proposed to address these drawbacks, including alloying, precipitation hardening, and ceramic particle reinforcement. Pillari et al. [1] developed B319-graphene composites and observed significantly reduced friction coefficients and improved wear resistance under dry sliding conditions. In a related study, the same research group [5] linked these improvements to the formation of a graphene-rich lubricating layer and microstructural refinement, enhancing both thermal conductivity

check for updates

Received: 16 May 2025
Revised: 26 May 2025
Accepted: 28 May 2025
Published: 29 May 2025

Citation: Tasci, U. Microstructure, Mechanical Strength, and Tribological Behavior of B_4C/WS_2-Hybrid-Reinforced B319 Aluminum Matrix Composites. *Lubricants* **2025**, *13*, 247. https://doi.org/10.3390/lubricants13060247

Copyright: © 2025 by the author. Licensee MDPI, Basel, Switzerland. This article is an open access article distributed under the terms and conditions of the Creative Commons Attribution (CC BY) license (https://creativecommons.org/licenses/by/4.0/).

and mechanical integrity. However, these studies focused primarily on tribological improvement through graphene-based lubrication, lacking a complementary hard-phase reinforcement to address mechanical strengthening. In contrast, the current study seeks to combine both strengthening and lubricating effects via a dual-reinforcement strategy. From a broader perspective, Singhal et al. [6] underlined that properly engineered aluminum matrix composites (AMCs) provide a unique combination of stiffness, wear resistance, and weight reduction, making them highly suitable for high-performance structural applications. While their work highlights the general potential of AMCs, it does not address B319 specifically or hybrid reinforcements that can overcome trade-offs between wear resistance and mechanical strength. Among reinforcing agents, boron carbide (B_4C) has received increasing attention due to its ultrahard nature, low density, and strong wear resistance, which make it ideal for structural reinforcement in lightweight composites. Karpasand et al. [7] produced Al7075-TiB_2-B_4C hybrid composites using friction stir processing. They reported significant improvements in hardness and tensile strength, attributing these enhancements to the reinforcements' uniform dispersion and complementary action. Similarly, Gorshenkov et al. [8] showed that including B_4C with ultra-dispersed tungsten particles refined the matrix microstructure and improved composite stability. Although these studies demonstrate the individual effectiveness of ceramic reinforcements, few have addressed the critical challenge of simultaneously enhancing both mechanical and tribological properties without sacrificing ductility or density. More recently, hybrid composites that combine hard reinforcements with solid lubricants have gained traction due to their potential to improve strength and tribological performance simultaneously [9]. In this context, tungsten disulfide (WS_2) has emerged as a promising solid lubricant reinforcement, characterized by its layered structure, chemical stability, and ability to form low-friction tribo-films on contact surfaces. Yuan et al. [10] examined the effect of WS_2 addition in self-lubricating coatings and demonstrated that it significantly reduced wear rates by forming a protective transfer film. Niste et al. [11] further reported that WS_2 based Al composites achieved superior lubrication performance and lower friction coefficients in dry sliding conditions, outperforming traditional lubricant systems. Although these studies establish WS_2 as an effective solid lubricant, they neither explored its interaction with ceramic phases like B_4C nor assessed its role in structural applications where mechanical integrity is as critical as wear resistance. However, these efforts largely exclude B319-based matrices, and no prior research has systematically investigated the synergistic use of B_4C and WS_2 within B319 alloys to address their concurrent deficiencies in strength and wear resistance. This gap is particularly significant when considering the unique potential of B_4C and WS_2 to complement each other—B4C contributing hardness and load-bearing ability, while WS_2 provides interfacial lubrication and fracture deflection. Thus, a systematic comparison of hybrid reinforcement versus traditional single-particle strategies is urgently needed to assess the feasibility of multifunctional enhancements.This gap is particularly significant when considering the unique potential of B_4C and WS_2 to complement each other—B_4C contributes hardness and load-bearing ability, while WS_2 provides interfacial lubrication and fracture deflection. Thus, a systematic comparison of hybrid reinforcement versus traditional single-particle strategies is urgently needed to assess the feasibility of multifunctional enhancements. Additionally, powder metallurgy (PM) has proven effective in producing MMCs with superior microstructural control and reinforcement distribution. Fogagnolo et al. [12] emphasized that mechanical alloying promotes homogeneous dispersion of reinforcements and enhances interfacial bonding, resulting in composites with improved strength and wear resistance. Süzer et al. [13] similarly demonstrated that high-entropy ceramic particulates uniformly integrated into Al matrices via PM result in dense, thermally stable, and mechanically robust composite structures.

This study presents the design, fabrication, and comprehensive characterization of novel B319/B_4C/WS_2 hybrid composites produced via hot-pressing powder metallurgy. Unlike conventional aluminum matrix composites, this research uniquely integrates 10 wt% B_4C and varying amounts of WS_2 (0.5 and 2 wt%) to achieve a synergistic enhancement of both mechanical strength and tribological performance. The novelty lies in the dual-action reinforcement approach explicitly tailored for B319's deficiencies, which has not been previously demonstrated in the literature. The hybrid reinforcement strategy aims to overcome the inherent trade-off between hardness and wear resistance by combining the load-bearing capability of B_4C with the solid lubricating properties of WS_2. Through systematic microstructural, mechanical, and wear analyses, the developed composites are demonstrated as promising candidates for advanced automotive, aerospace, and marine applications where simultaneous improvements in structural integrity, wear durability, and lightweight performance are critically required.

2. Experimental Procedure

2.1. Fabrication of B319/B_4C/WS_2 Hybrid Composite Specimens

B319 aluminum alloy powder (average particle size ~30 μm), boron carbide (B_4C, ≤5 μm), and tungsten disulfide (WS_2, ≤5 μm) powders were procured from Nanografi Nanotechnology™ (Ankara, Turkiye). Initially, a base composite material containing 10 wt% B_4C was prepared. Subsequently, hybrid composite powders were formulated by incorporating WS_2 known for its solid lubrication properties at concentrations of 0.5 and 2 wt% into the B319 + 10%B_4C matrix. The choice of 10 wt% B_4C was based on previous studies reporting that this reinforcement ratio significantly enhances mechanical properties without inducing notable agglomeration or processing challenges in aluminum matrix composites [14–16]. For WS_2, low concentrations were preferred by earlier research, which indicated that additions above 1 wt% often lead to particle clustering and localized porosity due to its layered morphology [17,18]. Informed by these findings and our previous experience with multi-phase powder processing, 2 wt% was selected as the upper limit to maximize tribological benefit while preserving microstructural integrity. To ensure homogeneous dispersion of the reinforcement particles (B_4C and WS_2) within the B319 matrix, a high-energy three-dimensional ball mixer was employed. The mixing process was conducted at 300 rpm for 4 h using a powder/ball weight ratio of 1:5. To prevent contamination during mixing, the powders were processed in a specialized plastic chamber using yttria-coated zirconia balls of two diameters (5 mm and 10 mm). Following homogenization, the blended powders were cold-pressed at 10 MPa into a mold made of hot work tool steel. The green compacts were then subjected to hot pressing under a uniaxial pressure of 350 MPa at 550 °C for 60 min, with a heating rate of 10 °C/min. The resulting compact blocks (dimensions: 40 × 40 × 10 mm^3) were machined using electrical discharge machining (EDM) to obtain specimens for microstructural analysis, hardness measurement, transverse rupture strength (TRS) testing, and wear characterization. Standard metallographic preparation procedures, including polishing and etching, were applied prior to characterization.

2.2. Microstructure and Mechanical Analysis

The grain size distribution of the blended composite powders was analyzed using a Malvern Mastersizer 3000 (Malvern, Worcestershire, UK) laser particle size analyzer. Microstructural characterization and compositional mapping were initially carried out using a TESCAN MAIA3 XMU (Tescan, Brno, Czechia) scanning electron microscope (SEM). For high-resolution imaging, elemental distribution, and energy-dispersive X-ray spectroscopy (EDS), a HITACHI SU8700 (Hitachi, Tokyo, Japan) field emission scanning

electron microscope (FE-SEM) was employed. Phase identification of the samples was performed via X-ray diffraction (XRD) using a Bruker D8 Advance (Bruker, Karlsruhe, Germany) diffractometer.

Microhardness testing followed the ASTM E384-17 standard [19], utilizing a HV0.5 load. Measurements were recorded at nine different positions across each specimen to obtain representative average values. Transverse rupture strength (TRS) was evaluated in accordance with the MPFI-41 standard [20] using an Instron MFL universal testing machine with a 200 kN load capacity. Tests were conducted at ambient temperature with a crosshead speed of 1 mm/min on samples with dimensions of $6.45 \times 12.7 \times 31.2$ mm^3.

Wear resistance was assessed through reciprocating wear tests based on ASTM G133-05 [21] using an Anton Paar TRB3 (Anton Paar, Graz, Austria) tribometer. All experiments were conducted at room temperature under a constant load of 5 N and a sliding distance of 100 m. The wear rate (ω) of composite materials can be calculated with the following equation using the area analysis determined by the 3D profilometer;

$$\omega = \frac{V}{L \times N} \quad (1)$$

where V is wear volume, L is sliding distance, and N is load.

3. Results and Discussion

3.1. Characterization of Starting Powder Materials

The morphological and phase characteristics of the B319 matrix alloy were analyzed using SEM (Tescan, Brno, Czechia) and XRD (Bruker, Karlsruhe, Germany) techniques, as illustrated in Figure 1. The SEM micrograph in Figure 1a reveals that the B319 alloy powder exhibits a uniformly spherical morphology, which is beneficial for powder flowability and densification during the compaction and sintering steps. Such spheroidal geometry also enhances homogeneity in reinforcement distribution. The corresponding XRD spectrum in Figure 1b identifies the presence of α-Al as the primary phase, along with secondary phases of Si and the intermetallic compound Al_2Cu, which are consistent with the typical phase constituents of B319 cast alloys [1,5]. The detection of these phases confirms that the alloy chemistry remains stable in the powder form, suitable for composite reinforcement processing.

The spherical morphology of B319 powders is particularly advantageous for powder metallurgy (PM) processing because it ensures higher packing density and minimizes the formation of interstitial voids during cold compaction and sintering. Additionally, the presence of intermetallic phases such as Al_2Cu and Si is crucial, as these phases act as hardening agents by impeding dislocation movement during subsequent mechanical loading. However, an excess amount or coarse morphology of these phases can become detrimental, promoting crack initiation sites. Therefore, maintaining a fine and uniform dispersion of these phases is critical for achieving optimized mechanical performance in the final composite.

Compositional analysis of the individual powder materials was conducted via FE-SEM coupled with EDS mapping. Figure 2 presents the elemental maps of the unreinforced B319 alloy, the B_4C ceramic particles, and the WS_2 solid lubricant. The B319 powder displays a uniform distribution of Al, Si, Cu, and trace Mg, verifying the alloy's multiphase nature. The B_4C particles are characterized by sharp-edged morphologies with homogeneous distributions of B and C, while WS_2 powders exhibit fine, granular features with clearly mapped W and S elements. This detailed elemental mapping confirms the chemical purity and morphological compatibility of the reinforcement particles with the aluminum matrix, which is critical for uniform dispersion and interfacial bonding.

Figure 3 illustrates the morphology, elemental distribution, and particle size analysis of the hybrid powder mixture containing B319 + 10 wt% B_4C + 2 wt% WS_2, processed using a high-energy 3D ball mixer. As shown in the mapping images, the reinforcement particles are finely and uniformly distributed around and on the surfaces of the B319 particles, with no visible signs of agglomeration. The elemental maps of Al, Si, Cu, C, B, and W further confirm the homogenous dispersion of both B_4C and WS_2 phases within the matrix. The particle size distribution curve indicates a volume-based median diameter (D_{50}) of 24.7 µm, which closely aligns with the size of the original B319 matrix powder. This suggests that the milling process did not significantly alter the particle morphology or induce fragmentation. The preservation of powder integrity throughout mixing is important for ensuring processability and uniform sintering behavior.

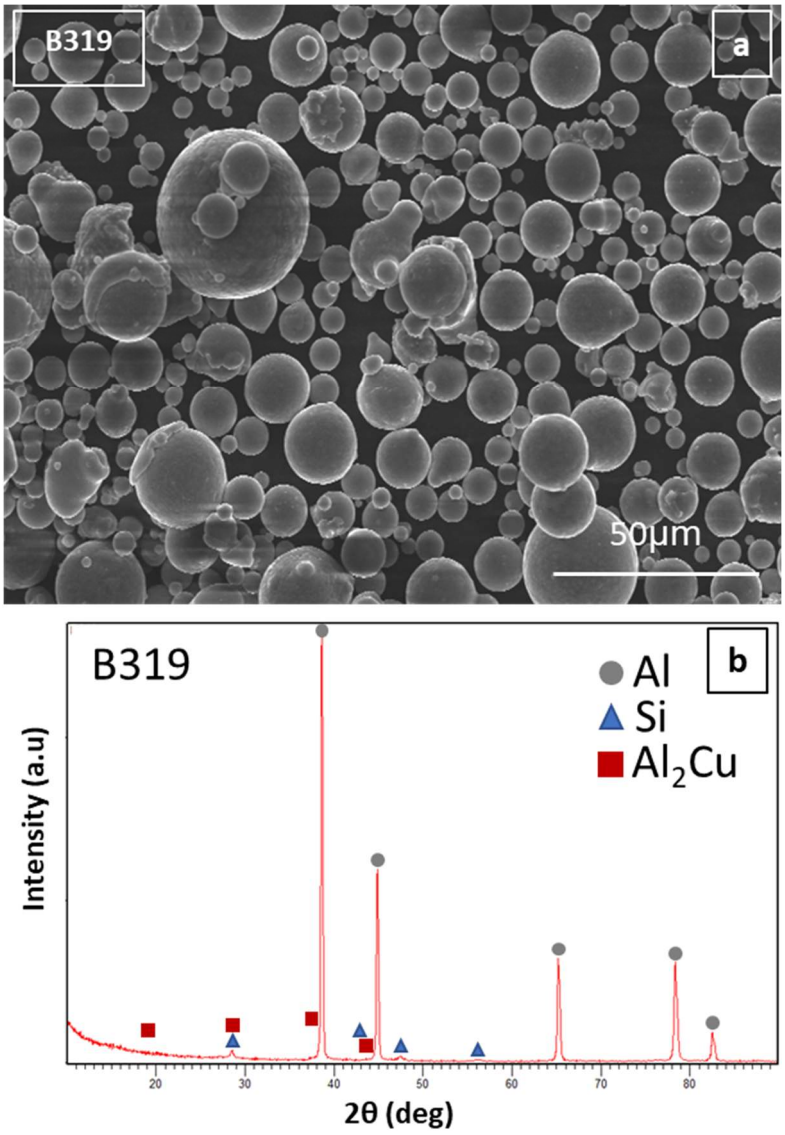


Figure 1. (**a**) SEM image of B319 alloy powder, (**b**) XRD pattern.

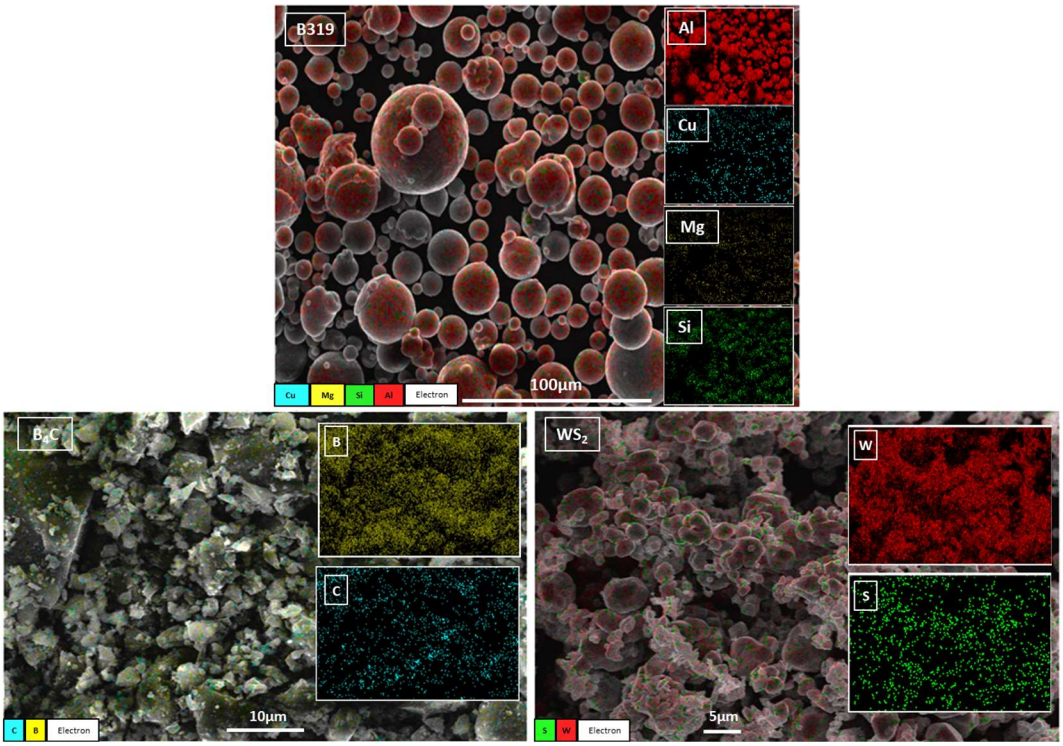


Figure 2. FE-SEM and EDS mapping of starting powders: B319 matrix, B_4C, and WS_2.

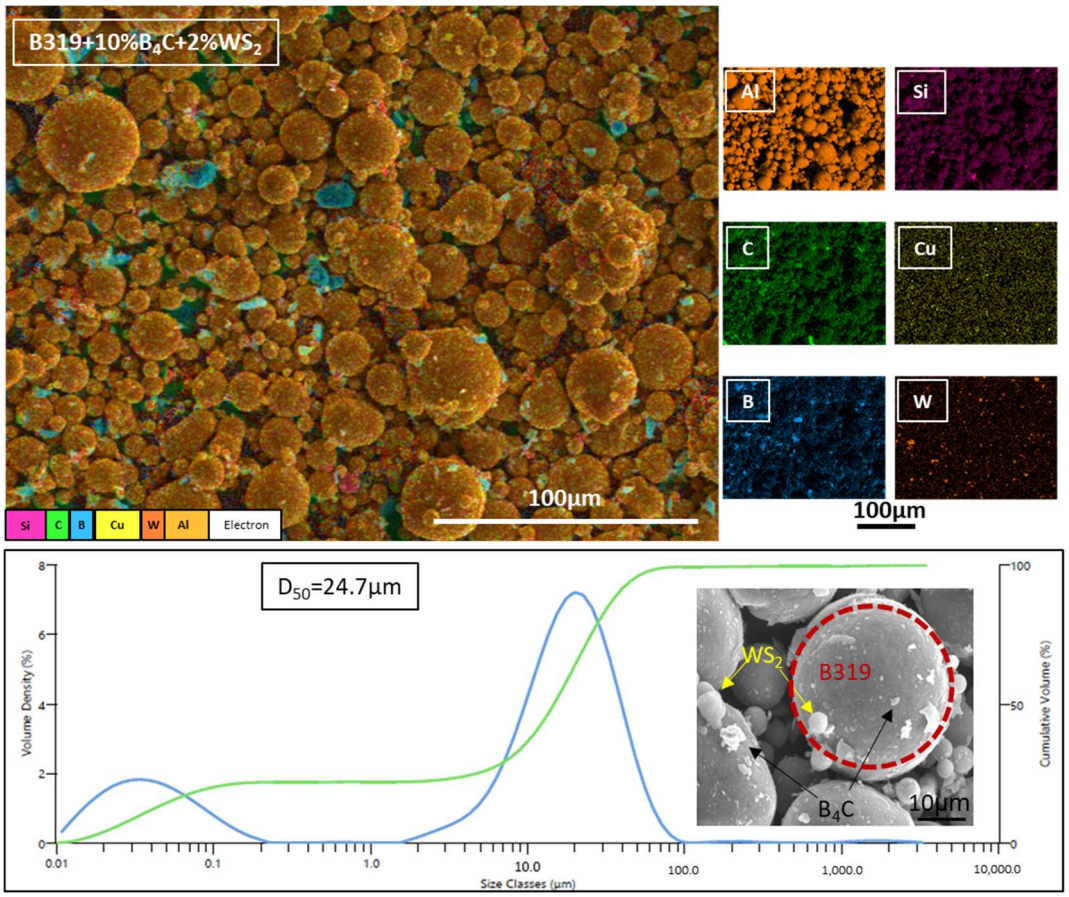


Figure 3. SEM image, element maps, and particle size distribution (D_{50} = 24.7 µm) of B319 + 10%B_4C + 2%WS_2 hybrid powder.

The effectiveness of the 3D ball milling approach in achieving homogeneous dispersion is evident and aligns with findings from similar studies in the literature [22]. Unlike conventional mixing methods that often suffer from clustering or inadequate wetting of reinforcements [23], this approach enables efficient mixing while maintaining the particulate structure. The resulting uniform reinforcement distribution is expected to facilitate better compaction, reduced porosity, and improved tribological and mechanical properties in the final sintered composite [24]. It is noteworthy that a uniform and fine distribution of B_4C and WS_2 at the powder stage plays a pivotal role in determining the microstructural integrity of the sintered composites. Well-dispersed hard B_4C particles act to hinder plastic deformation under load, while WS_2 particles, by their lamellar structure, promote the formation of continuous tribo-films during sliding, thereby improving wear resistance. Furthermore, maintaining a particle size comparable to the original matrix powder ensures minimal differential sintering shrinkage, thus reducing the risk of microcrack formation at reinforcement–matrix interfaces. This powder-level control is therefore fundamental for achieving the desired balance between mechanical strength and tribological performance in the hybrid composites.

3.2. Microstructure Characterization of Materials

Figure 4 illustrates the FE-SEM micrographs along with corresponding elemental mapping of the unreinforced B319 aluminum alloy. The microstructure reveals the presence of characteristic intermetallic and secondary phases, including eutectic Si, blocky Al_2Cu, and $Al_{15}(Fe, Mn)_3Si_2$ compounds. These findings are consistent with the literature on cast B319 alloys [1,25]. The Si phase appears as rod- or needle-like structures, while Al_2Cu is seen in irregular polygonal morphologies. The presence of $Al_{15}(Fe, Mn)_3Si_2$ phases is confirmed in both needle-like and angular geometries.

These intermetallics are typically formed during solidification and sintering due to the segregation of solute elements at grain boundaries. Their morphology and distribution are known to significantly affect the mechanical performance of the alloy, especially in terms of strength and fracture behavior [26]. Specifically, the coarse and brittle morphology of eutectic Si and Al_2Cu phases acts as potential crack initiation sites under mechanical loading, thereby compromising toughness. Conversely, a finer and more homogeneously distributed intermetallic network could enhance strength by impeding dislocation motion [27]. The observed microstructure of the unreinforced B319 suggests that, without additional reinforcement, the alloy may be susceptible to localized failure due to the stress concentration around these intermetallics, particularly during high-load or impact applications. Therefore, introducing well-dispersed reinforcements like B_4C and WS_2 becomes critical to mitigate these inherent microstructural weaknesses.

Figure 5 presents the FE-SEM and EDS mapping results of the B319 + 10wt% B_4C composite. The B_4C reinforcement particles appear well distributed within the aluminum matrix, with no signs of clustering or significant porosity around the particles. The mapping confirms the presence of B, C, and Si elements homogeneously dispersed throughout the matrix. The well-bonded and discrete nature of the B_4C particles indicates the effectiveness of both the 3D mixing and hot pressing parameters. The sharp contrast between reinforced and matrix regions suggests that the B_4C particles act as microstructural obstacles to dislocation motion, contributing to increased hardness and strength, as observed in similar composite systems [28]. The incorporation of B_4C particles leads to a dual strengthening mechanism: (i) grain refinement by impeding grain boundary mobility during sintering, and (ii) the Orowan strengthening effect, where the hard particles block dislocation motion, thus elevating the yield strength. Additionally, the absence of interfacial porosity suggests strong metallurgical bonding between the matrix and B_4C, which is critical for efficient

load transfer during mechanical stressing. This homogeneous microstructure is expected to significantly enhance not only hardness but also fracture resistance by promoting crack deflection and energy absorption mechanisms around the hard particles.

Figure 6 shows the FE-SEM microstructure images of the B319 + 10%B4C + 2%WS2 hybrid-reinforced composite material and the EDS elemental mapping analysis. When the FE-SEM images were examined, it was determined that both B_4C and WS_2 reinforcement particles showed a homogeneous distribution in the matrix, and no structural irregularities such as clustering or regional agglomeration were observed. This observation indicates the effectiveness of three-dimensional powder mixing and hot pressing processes in providing homogeneous particle distribution. The high-magnification FE-SEM images determined that the polygonal and hard-structured B_4C particles were observed to be well-bonded with the matrix in places within the matrix; the WS_2 particles were embedded in the surface with their layered structures. The EDS mapping results show that Al, Si, B, C, W, and S are distributed homogeneously throughout the surface. While the B and C signals correspond to the B_4C particles, the distribution of the W and S elements confirms the WS_2 particle reinforcement. In addition, the continuous and stable distribution of Al and Si elements indicates that the main matrix maintains its chemical integrity [11,29].

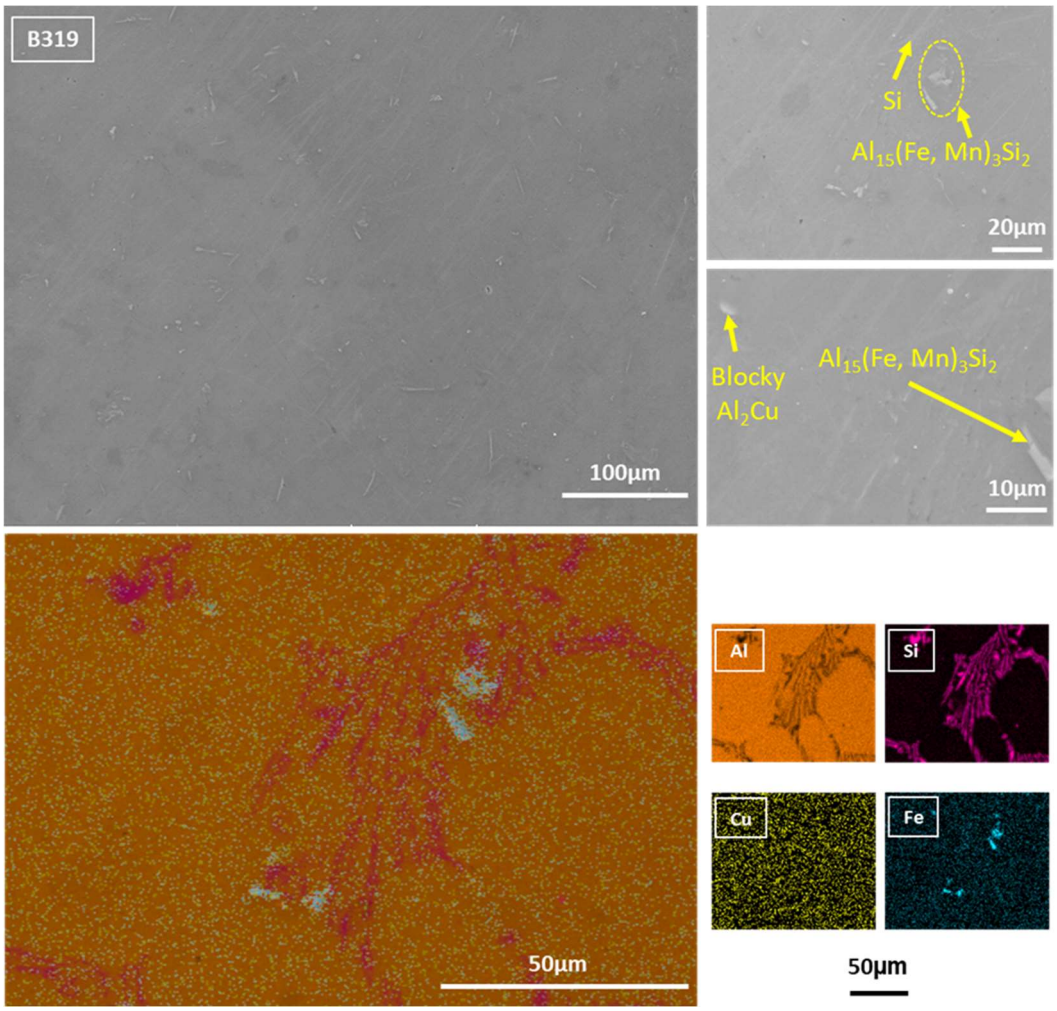


Figure 4. FE-SEM and elemental mapping of unreinforced B319 material.

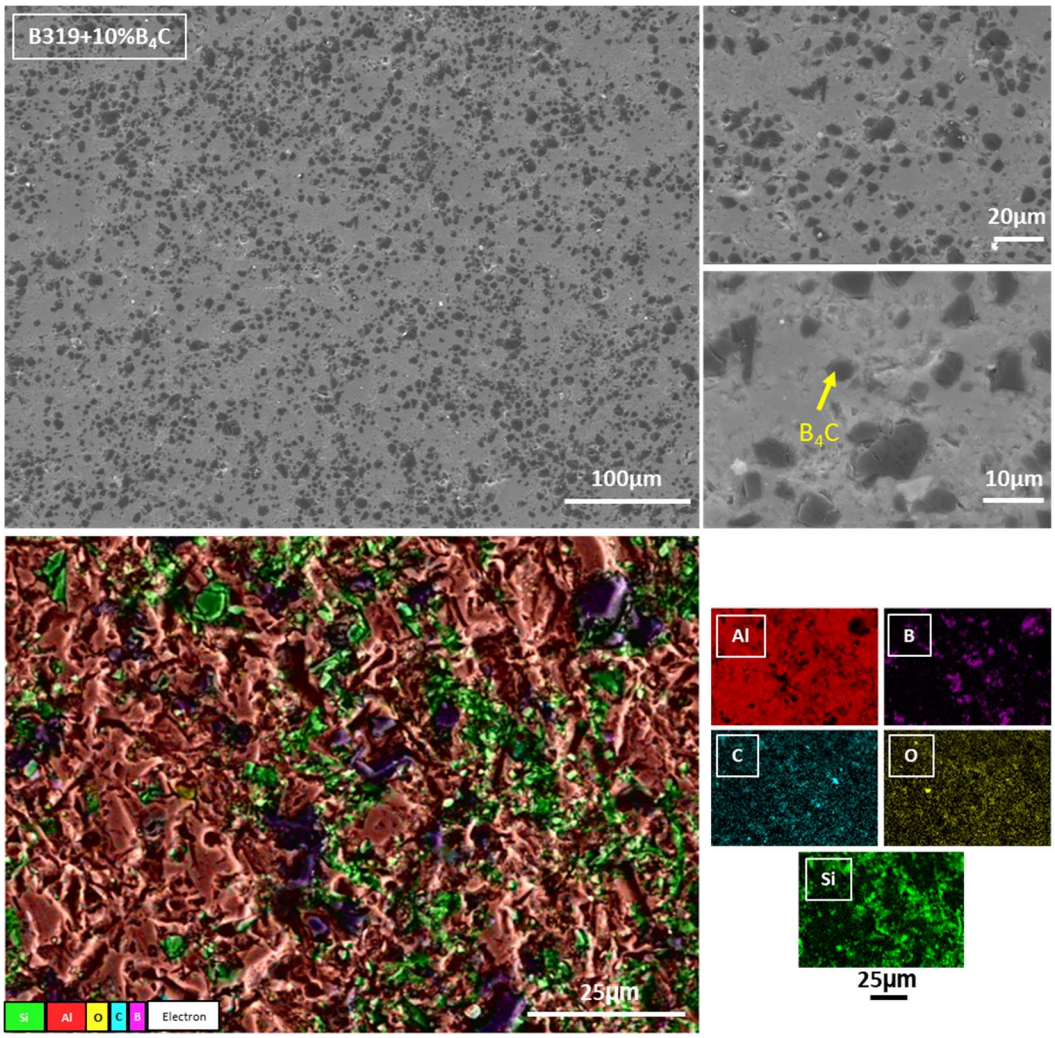


Figure 5. Microstructure and EDS mapping of B319 + 10%B_4C composite material.

The WS_2 appears to play a complementary role to B_4C by providing solid lubrication properties while simultaneously reinforcing the matrix. Moreover, the addition of WS_2 contributes to a hybrid reinforcement effect, where the hard B_4C particles mainly enhance mechanical strength, while the WS_2 phase introduces intrinsic solid lubrication properties by forming a tribo-film under sliding conditions. From a microstructural perspective, WS_2's presence near B_4C particles may further reduce localized stress concentrations by promoting stress redistribution around potential crack initiation sites. The overall refined and defect-free microstructure thus suggests improved synergy between strength and tribological performance, offering a balanced enhancement critical for structural applications subjected to both static and dynamic loading.

3.3. Physical and Mechanical Properties

Figure 7 presents the relative density and Vickers microhardness (HV0.5) measurements of the produced specimens. Among all samples, the unreinforced B319 alloy showed the highest relative density at 99.1%, yet it recorded the lowest hardness value of 80.5 HV. In contrast, the hybrid composite with 10 wt% B_4C and 2 wt% WS_2 showed the highest hardness (104.3 HV), indicating a ~30% increase [30]. The observed decrease in relative density with increasing reinforcement content (especially WS_2) can be attributed to the inherent difficulty in densifying ceramic and lubricating particles during sintering. However, this slight compromise in density is outweighed by the significant gain in hardness,

indicating improved load-bearing capacity due to uniform particle dispersion and strong interfacial bonding [31,32].

The increase in hardness can be primarily attributed to the Orowan strengthening mechanism and the load-bearing effect introduced by the hard B_4C particles. The presence of WS_2 further contributes to mechanical strengthening by reducing interfacial shear stress and preventing premature microcrack initiation under applied loads. Although the slight decrease in density might raise concerns about porosity, the uniform dispersion and strong bonding observed in microstructural analyses suggest that the reinforcement phases are effectively embedded, minimizing their adverse impact on mechanical properties. Moreover, the enhanced hardness is expected to directly translate into better wear resistance and improved structural reliability under cyclic loading conditions, as also observed in similar hybrid composites [33]. Although a slight decrease in relative density was observed with the increase in WS_2 content, this did not lead to a significant decrease in microhardness values. On the contrary, the composites' hardness improved steadily with the incorporation of B_4C and WS_2, indicating that the reinforcing effect and interface bonding mechanisms effectively compensated for the small porosity introduced during sintering. These findings indicate that the degree of densification achieved was sufficient to maintain mechanical stability in hardness [34,35].

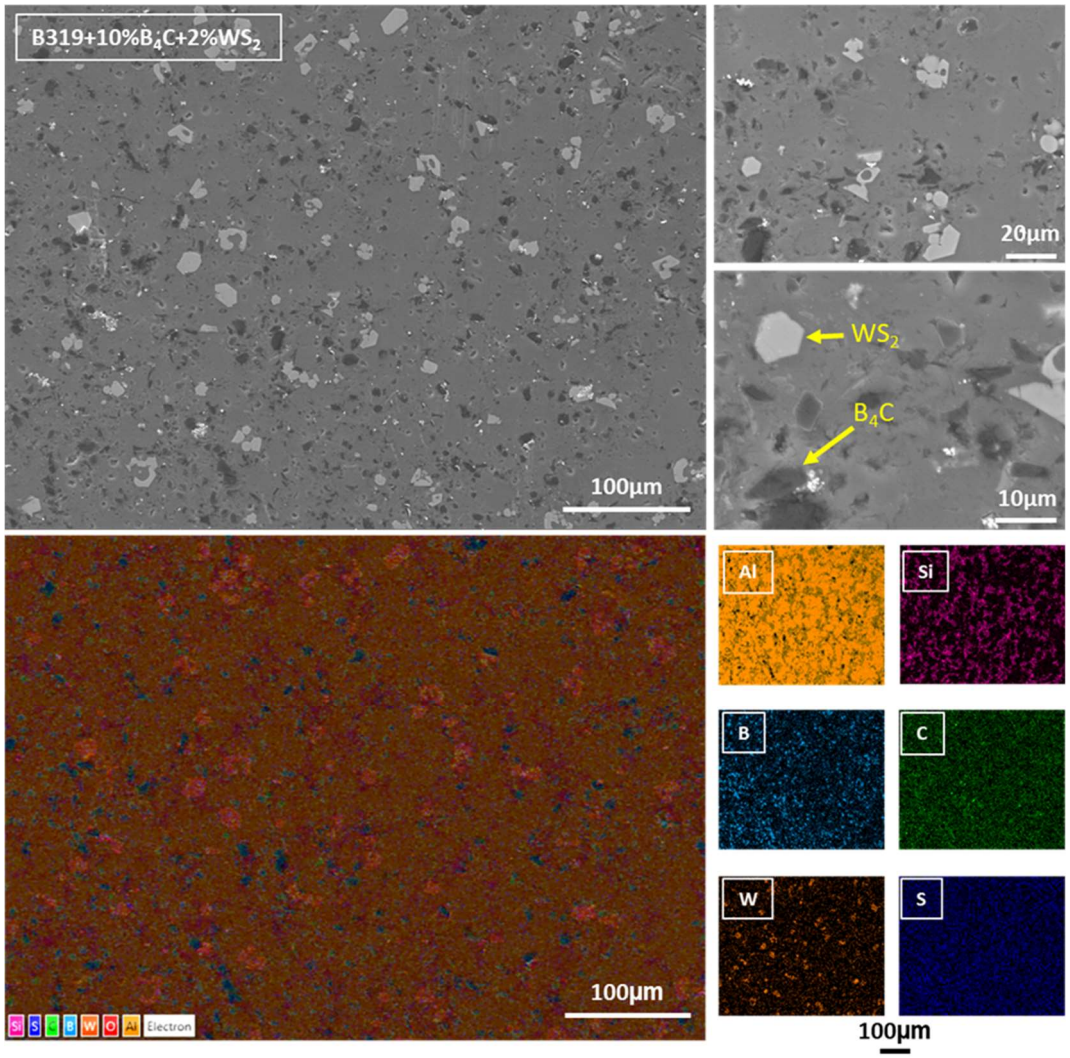


Figure 6. FE-SEM and elemental mapping analysis images of B319 + 10%B_4C + 2%WS_2 composite material.

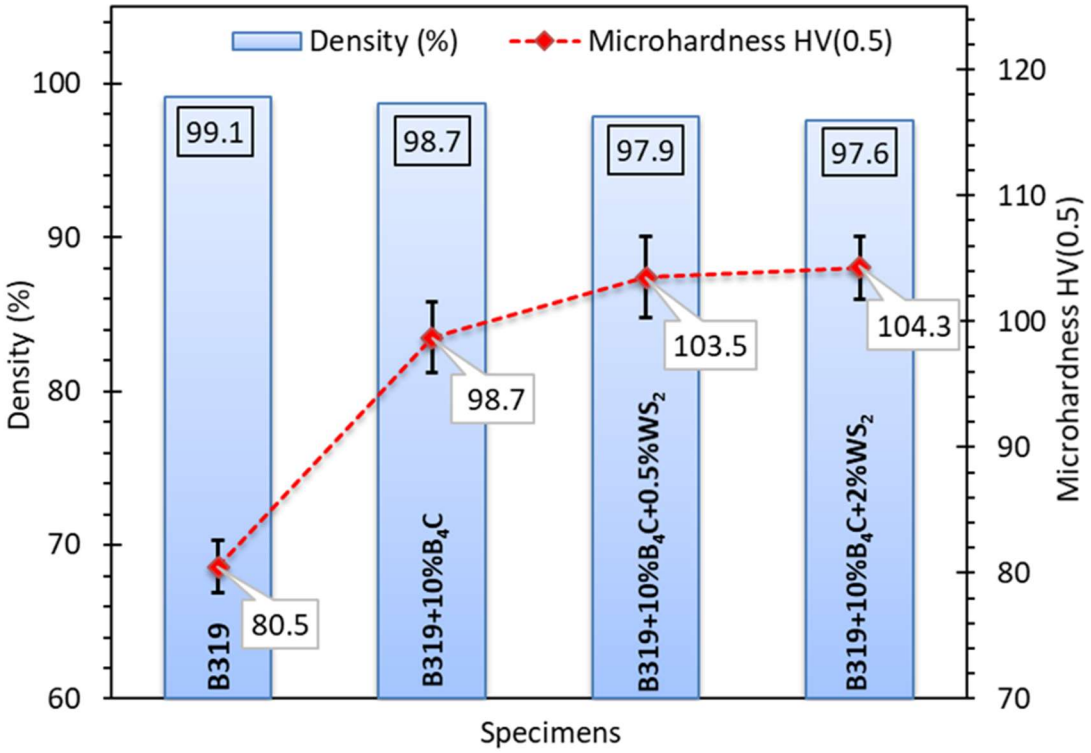


Figure 7. Relative density and Vickers microhardness of B319 alloy and reinforced composites.

3.4. Transverse Rupture Strength Analysis

Transverse rupture strength (TRS) results are displayed in Figure 8. The B319 alloy reached a TRS of 163.8 MPa, while the B319+10%B4C composite increased to 178.5 MPa. The highest TRS was recorded for the hybrid composite containing 2% WS2, reaching 196.3 MPa an improvement of approximately 20% compared to the base alloy. This improvement is attributed to the crack-blocking capability of the rigid B4C particles combined with the energy-absorbing nature of WS2, which together act to hinder crack propagation and enhance structural integrity. These reinforcements effectively improve strength and toughness under bending stress [36].

The enhancement in TRS can be explained by the dual action mechanism where B_4C particles increase the intrinsic strength of the matrix by serving as crack arresters and stress redistributors, while WS_2 particles contribute to energy dissipation during crack propagation. In hybrid composites, the toughening effect of WS_2 complements the hardening effect of B_4C, leading to a balanced improvement in both strength and ductility. Such a synergistic behavior is particularly advantageous in bending or flexural applications where resistance to crack initiation and stable crack growth are critical for component longevity [20].

The SEM fracture surface images in Figure 9 provide important findings in explaining the fracture behaviors occurring in B319 alloy and composites with different reinforcement configurations after TRS tests at the microstructural level. The B319 alloy without reinforcement exhibited a largely brittle fracture behavior. The fracture surface morphology shows distinct grain boundary separations, intergranular cracks, and planar cleavage marks. These observations indicate that the matrix has limited capacity against plastic deformation, and the fracture mainly progresses at the grain boundaries. In addition, the sharp and irregularly shaped eutectic Si phases frequently encountered in Al-Si alloys cause local stress concentrations and have a crack-initiating effect, increasing brittleness [37].

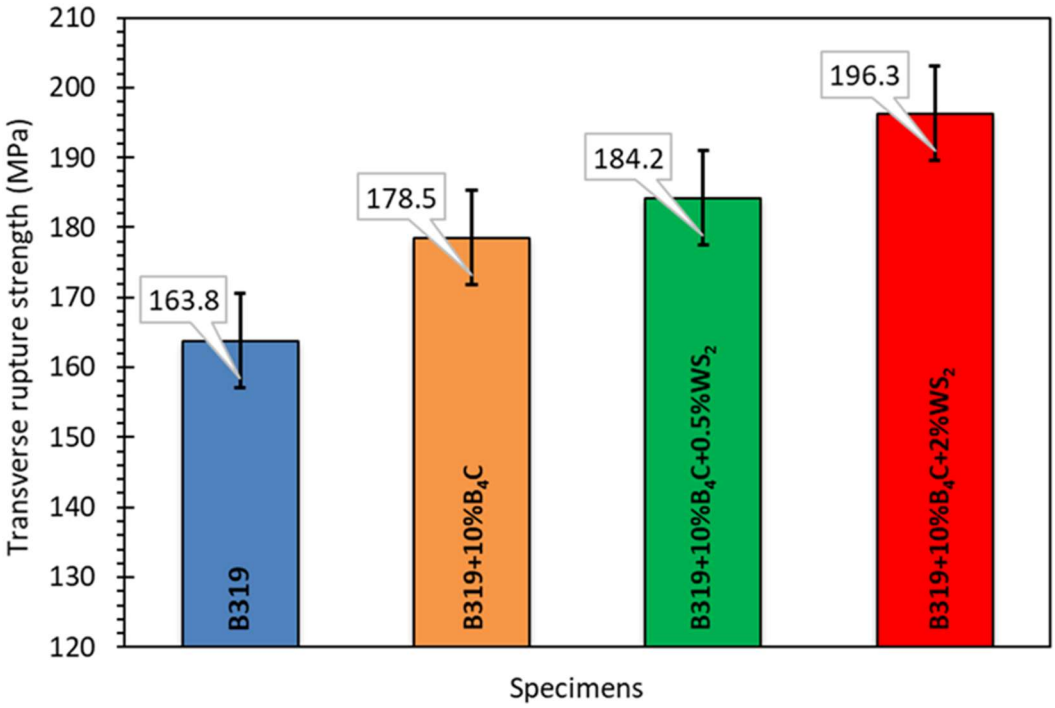


Figure 8. Transverse rupture strength of unreinforced and reinforced composites.

The fracture surface morphology of the B319 + 10%B_4C composite material became more complex, and mixed-mode fracture was observed. The hard ceramic particles increased the overall mechanical strength by increasing the load transfer between the matrix, but at the same time, resisted crack propagation. The SEM images show both flat surfaces indicating brittleness and small dimples indicating limited ductile deformation. It is thought that the cracks on the fracture surface deviate around the hard B_4C ceramic particles and change direction, thus making crack propagation difficult [38,39].

In the B319 + 10%B_4C + 0.5%WS_2 hybrid composite, the fracture surface morphology showed more ductile fracture signs. In particular, shallow but widely distributed dimples were observed on the surface, indicating that local plastic deformation began during crack propagation. There were still some cleavage marks and brittle areas on the fracture surface, indicating that the fracture mechanism had not become completely ductile. It is thought that the WS_2 particles slowed the crack propagation and increased the energy absorption capacity by forming shear planes during deformation [10,11]. However, this effect was thought to be limited due to the 0.5% reinforcement ratio.

In the hybrid composite reinforced with 2% WS_2 by weight, the morphology on the fracture surfaces showed a clear transition to a more ductile fracture behavior. Densely distributed, deeper, and regular dimple structures in SEM images are remarkable. In addition, it was observed that the planar cleavage marks decreased significantly, the crack propagation directions changed frequently, and the fracture surface became more irregular. This situation shows that plastic deformation became more effective, and the matrix gained a more resistant structure against crack propagation with an increased WS_2 particle reinforcement ratio [40]. The fracture surfaces are thought to contain dense and deep dimples without obvious cleavage planes. WS_2 reinforcement delayed the propagation by changing the crack paths, and significant plastic deformation occurred before fracture. The reinforcement WS_2 particles reduce local stress concentrations, prevent crack propagation by promoting homogeneous plastic flow, and delay crack coalescence during the test. These mechanisms contributed to the increase in overall fracture toughness. Additionally, the absence of continuous cleavage planes indicates that the 2% WS_2-reinforced hybrid

structure can absorb higher fracture energy and increase its usability under impact/loading conditions [41].

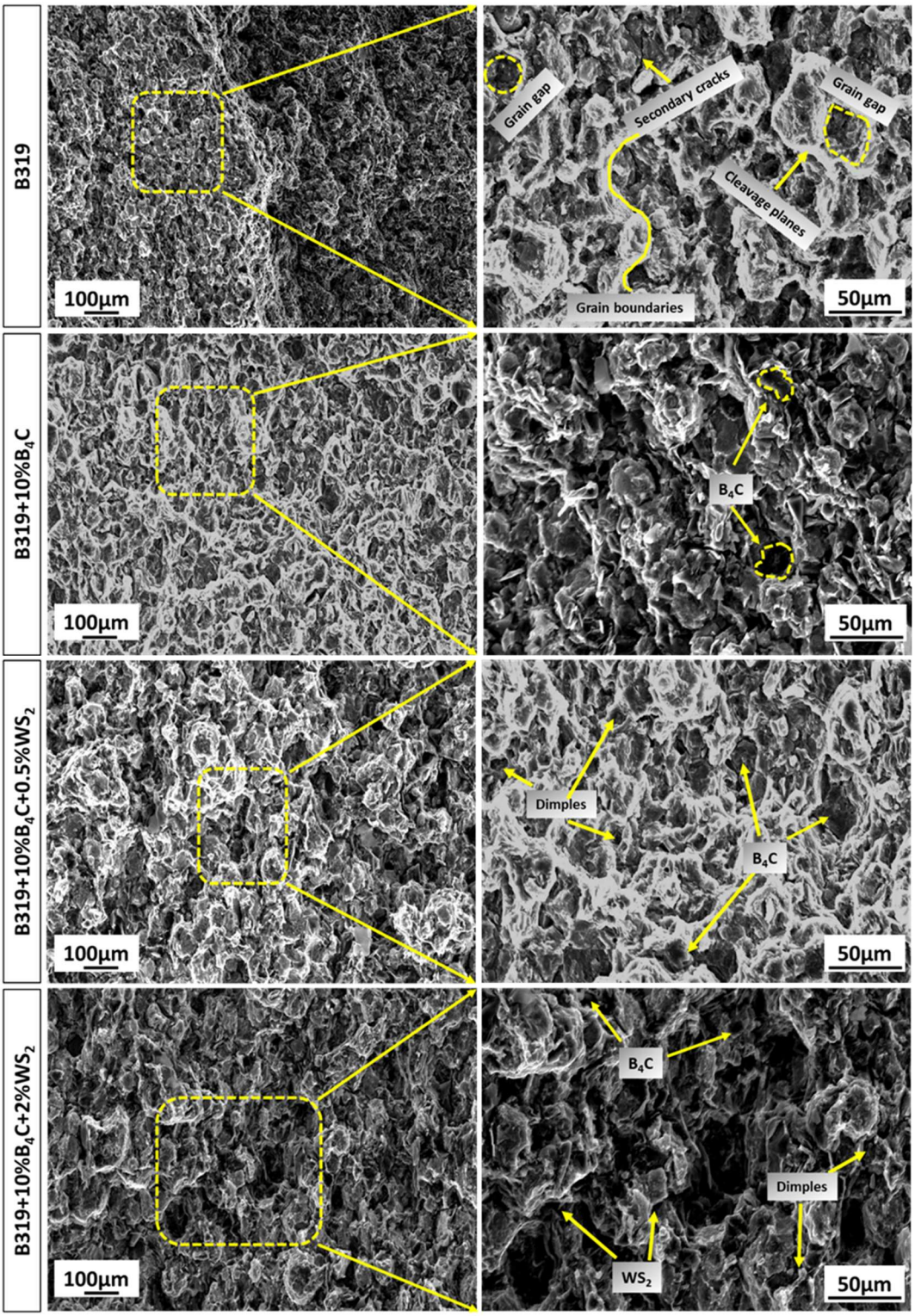


Figure 9. FE-SEM fracture surface images of samples after TRS testing.

3.5. Frictional and Wear Analysis

Figure 10 presents the weight loss and specific wear rate (SWR) values of the unreinforced B319 alloy and its composite/hybrid counterparts following wear tests conducted under a 5 N load. Both parameters exhibit a decreasing trend with the addition and increas-

ing content of reinforcement compared to the base alloy. The highest weight loss (0.0721 g) and specific wear rate of 5.48 × 10^{-5} mm^3/N·m showed the lowest wear performance. The composite material with 10% B_4C reinforcement increased wear resistance compared to B319 alloy material with 0.0544 g and 4.13 × 10^{-5} mm^3/N·m values. In the hybrid composites containing WS_2 ceramic reinforcement, a lubricant effect was observed, and especially the lowest weight loss (0.0057 g) and SWR (4.34 × 10^{-6} mm^3/N·m) values were obtained in the material containing 2% WS_2 reinforcement. This is mainly due to the formation of a lubricating WS_2-based film that reduces friction and improves surface durability [10]. This effect is well-documented in the literature, where WS_2 forms a lamellar tribo-film that minimizes direct metal-to-metal contact, lowers interfacial shear, and enhances surface stability during reciprocating motion [11].

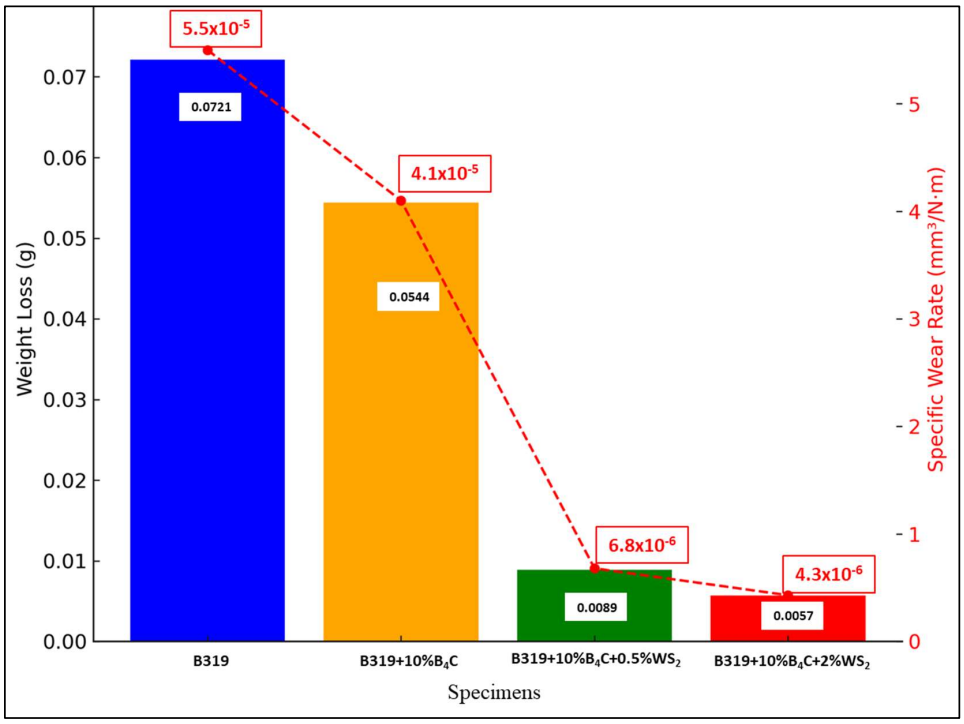


Figure 10. Graph of weight loss and specific wear rate of B319 alloy and hybrid/composite materials.

The significant reduction in both weight loss and SWR with increasing WS_2 content highlights the dual functional role of WS_2 particles. First, WS_2 acts as a solid lubricant, forming a low-shear tribo-film that reduces frictional heating and surface damage during sliding. Second, it enhances load distribution across the surface by filling micro-voids and smoothing asperity contacts. Meanwhile, the hard B_4C particles improve the load-bearing capacity of the matrix by resisting plastic deformation. It changes the dominant wear mechanism between B_4C and WS_2 in the matrix from severe adhesive and delamination wear (in unreinforced B319) to mild abrasive and lubricated wear in hybrid composites. Such a transformation is crucial to extend the service life of components under dynamic loading and mutual friction conditions [42].

Figure 11 illustrates the variation in friction coefficient (CoF) with sliding distance for unreinforced B319 and its reinforced composite samples. To isolate the effect of B_4C and B_4C/WS_2 hybrid reinforcements on the tribological performance, all testing conditions were maintained constant. The results indicate that the incorporation of 10% B_4C leads to a noticeable reduction in the friction coefficient compared to the base alloy, with a further decline observed in the hybrid composites containing WS_2. It was determined that the friction coefficient decreased to an average of 0.497 μ in the unreinforced B319 material and

an average of 0.381 μ in the B319 + 10% B_4C composite material. The hybrid-reinforced composite materials decreased, reaching the lowest value of 0.5%WS_2 reinforcement (0.215 μ) and 0.178 μ in the 2%WS_2-reinforced material [43]. This significant decrease in the friction coefficient value is associated with forming a transfer film layer on the surface because WS_2 mainly acts as a solid lubricant. This situation has also been stated in the literature, where WS_2 reinforced into the aluminum matrix significantly reduces the friction coefficient and forms a film as a solid lubricant [11,44]. Moreover, studies have shown that the effectiveness of this tribo-film increases with WS_2 concentration, leading to improved frictional stability under repeated sliding cycles.

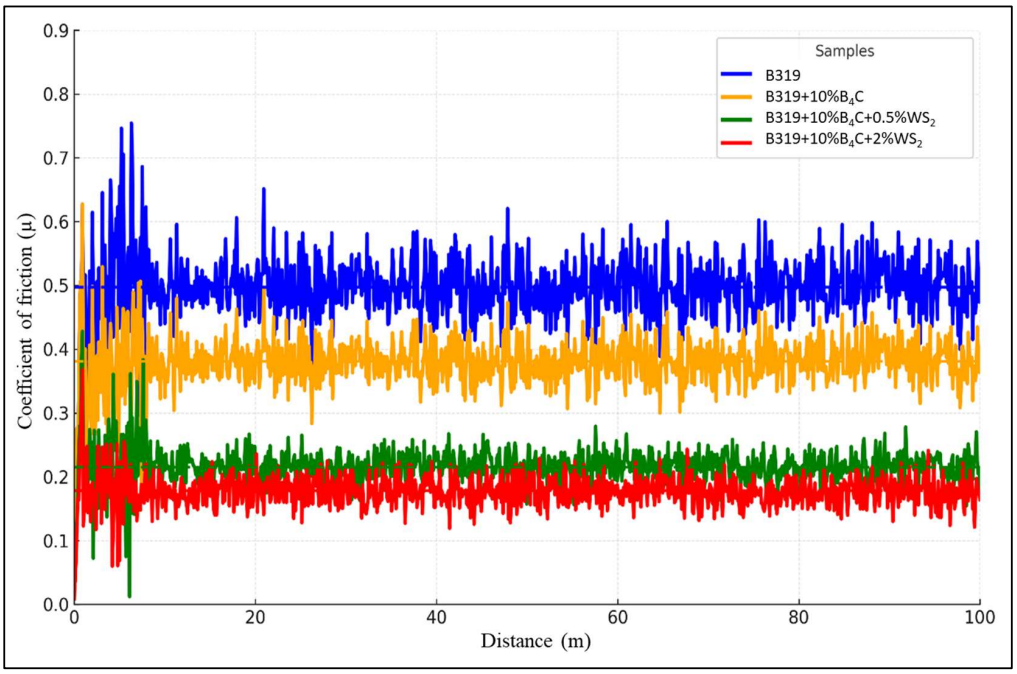


Figure 11. Graph of coefficients of friction of B319 alloy and hybrid/composite materials.

The progressive decline in CoF with increasing WS_2 content supports the hypothesis that WS_2 not only reduces adhesive forces between the sliding surfaces but also stabilizes the tribological interface by creating a continuous, low-shear film. This behavior prevents the formation of micro-welds and reduces the propensity for material transfer and seizure. In hybrid composites, the simultaneous presence of hard (B_4C) and lubricating (WS_2) phases ensures that the surface maintains high wear resistance while minimizing energy loss due to friction. This dual-functionality is particularly advantageous for applications requiring low-friction and high-durability materials under oscillating contact conditions [45,46].

Figure 12 shows the SEM analysis images of the worn surfaces of unreinforced B319 alloy and hybrid/composite materials after the reciprocating wear test. When the wear surface morphology of the unreinforced B319 alloy was examined in detail, it was determined that there were microcracks and delamination marks, especially with distinct scratch marks extending parallel to the friction direction. These structures show that wear is mainly based on adhesion and delamination mechanisms [47]. It was determined that due to excessive local temperature increase and pressure during the wear test, the particles that broke off from the surface adhered to the surface again, which caused smearing and material pull-out marks on the surface. Such wear surface marks indicate that the temporary tribo-film layer formed by the effect of local plastic deformation under load was weak and discontinuous. However, the obtained data suggest that this film layer is not stable and protective; instead, it is thought to break down under high deformation and promote wear easily. Microcracks

on the surface indicate that the crack tips progressed due to the cyclic tension and relaxation effect during friction and that the surface disintegrated over time due to thermomechanical fatigue. Observed adhesive wear zones indicate that complex processes such as short-term oxidation and surface reattachment occurred during contact [48].

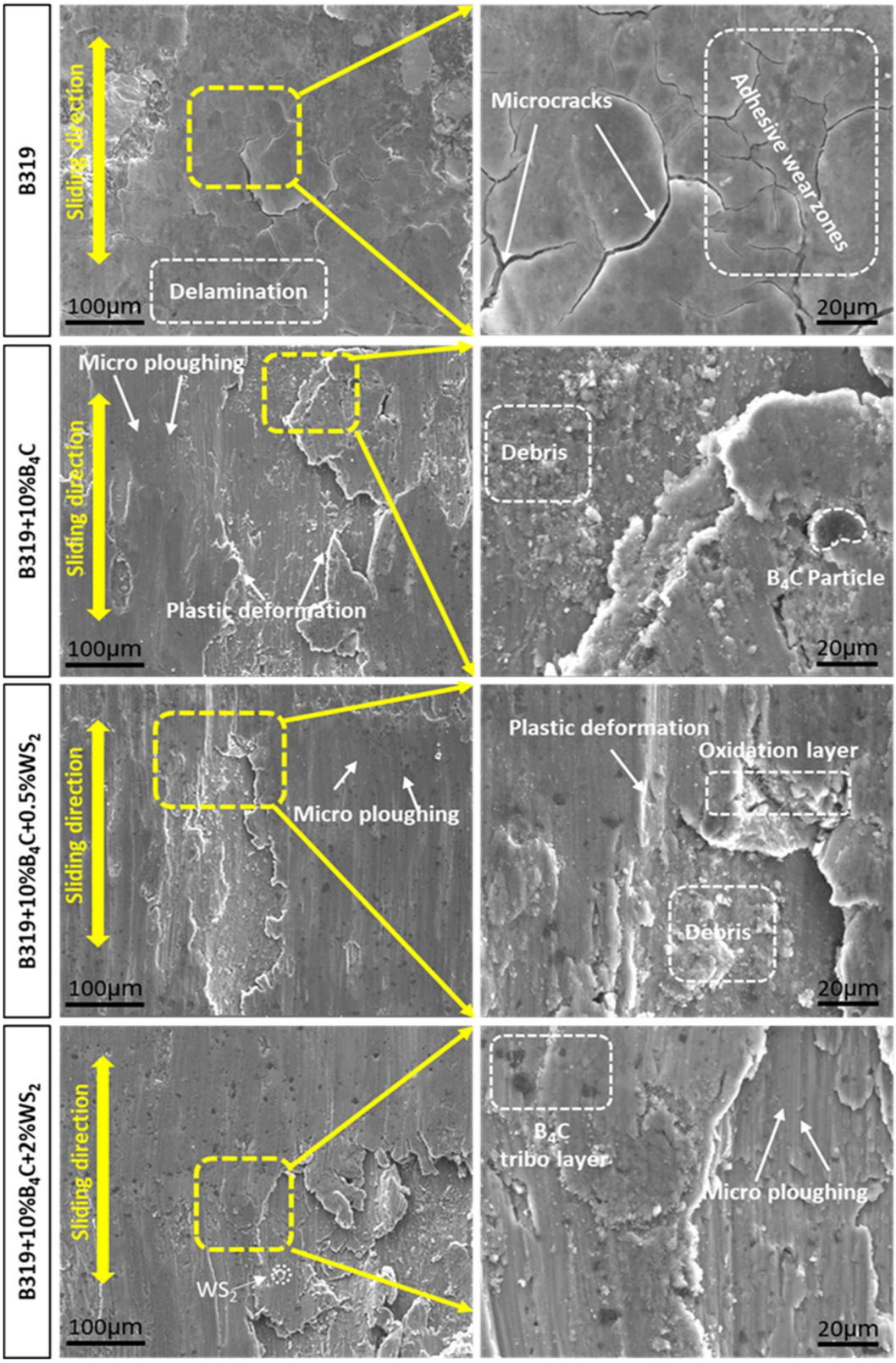


Figure 12. Graph of worn surfaces analysis of B319 alloy and hybrid/composite materials.

When the surface morphology of the B319 + 10%B_4C composite material was examined, micro-ploughing, evident plastic deformation traces, widespread particle debris, and B_4C reinforcement particles embedded in the surface were observed. The observed wear behaviors indicate the presence of an abrasive wear mechanism. The scratch structures and deformation traces on the surface reveal that the reinforcement particles enter the contact area during friction and create a cutting effect. This effect leaves directed traces along the surface. In particular, the high hardness of B_4C particles is thought to act as micro-cutters against the surface, reducing the plastic deformation threshold and locally intensifying the surface wear. However, it was determined in the image that some B_4C particles tend to leave the matrix and break off, which leads to additional debris and scratches on the surface [49].

The wear surface of the B319 + 10%B4C + 0.5%WS2 hybrid composite material shows that the wear behavior in the hybrid structure created with WS_2 and B_4C additives is shaped by both mechanical effects and limited physical changes occurring on the surface. The friction coefficient was decreased with 0.5% WS_2 reinforcement in the matrix. This situation is related to the fact that WS_2 particles, thanks to their structure that can easily slide between layers with low shear stress, reduce the real contact area by acting as a solid lubricant film in the contact between the surfaces, making the load transfer more homogeneous and minimizing the surface friction at the microscopic level [50].

When the surface morphology of the B319 + 10% B_4C + 2%WS_2 hybrid composite material was examined after wear, it was observed that the deformation depth on the surface decreased significantly compared to the other samples, the micro-ploughing marks became more regular, and the tribo layers of B_4C were more pronounced on the surface [31,51]. This structure shows that the B_4C particles played a mechanical balancing role in the contact area during wear and created a protective effect on the surface. It was determined that the deep scratches and surface cracks observed on the wear surface decreased with the increase of 2% WS_2 reinforcement. This situation shows that the friction-suppressing effect of WS_2 between the surfaces became more effective. In addition, it is understood that the wear marks exhibited a directional and parallel distribution, and the elastic-plastic deformation behavior dominated the surface thanks to the smooth and sliding surfaces formed by WS_2. This observed situation reveals that the surface can carry loads without experiencing severe delamination and thus provides an advantage in terms of long-term wear resistance [52]. Thanks to the effect of B_4C and WS_2 reinforcements, the wear behavior in the hybrid structure developed mainly in the form of controlled micro-ploughing and regular surface sliding, and it was determined that the material surface resisted wear homogeneously [53]. This effect is directly related to the decrease observed in the coefficient of friction (CoF) and specific wear rate (SWR) values. In particular, the increase in WS_2 content led to a transition to a more stable wear mechanism. It was observed that surface deformations remained more superficial, microscopic cracks and particle breakages were minimized, and surface integrity was maintained for a longer time thanks to the 2% WS_2 ratio [54].

Figure 13 illustrates the FE-SEM/EDS line scan analysis of the worn surface of the B319 + 10%B_4C + 0.5%WS_2 hybrid composite. The scan was conducted across the wear track, and elemental distributions for Al, Si, O, B, C, W, and S were evaluated. The matrix elements, particularly Al and Si, exhibit a uniform distribution along the scanned path, indicating the structural consistency of the aluminum alloy substrate. A notable increase in oxygen content was observed within the wear groove, which can be attributed to oxidative reactions occurring due to frictional heating during sliding. Additionally, the elements corresponding to the reinforcement phases, B (from B_4C), W, and S (from WS_2), were detected along the groove area, confirming their active involvement in the tribological interaction zone. The continuous presence of W and S along the track suggests

the formation of a WS_2-based tribo-film. This tribo-film likely contributed to the reduced friction coefficient and improved wear resistance, as it acts as a solid lubricant layer between the contact surfaces [11,55]. The detection of W and S signals across the wear track provides direct evidence for the in-situ formation of a WS_2 tribo-film during sliding [56]. Such a film serves two critical functions: (i) it minimizes direct metallic contact, thereby reducing adhesive wear, and (ii) it stabilizes the frictional interface, promoting smoother sliding and lowering shear stresses. The elevated oxygen levels detected in the groove further suggest that oxidative wear, while present, is effectively mitigated by the protective tribo-film [57]. This combined behavior aligns well with the observed improvements in CoF and SWR values, reinforcing the critical role of WS_2 in enhancing surface durability under reciprocating loads [58].

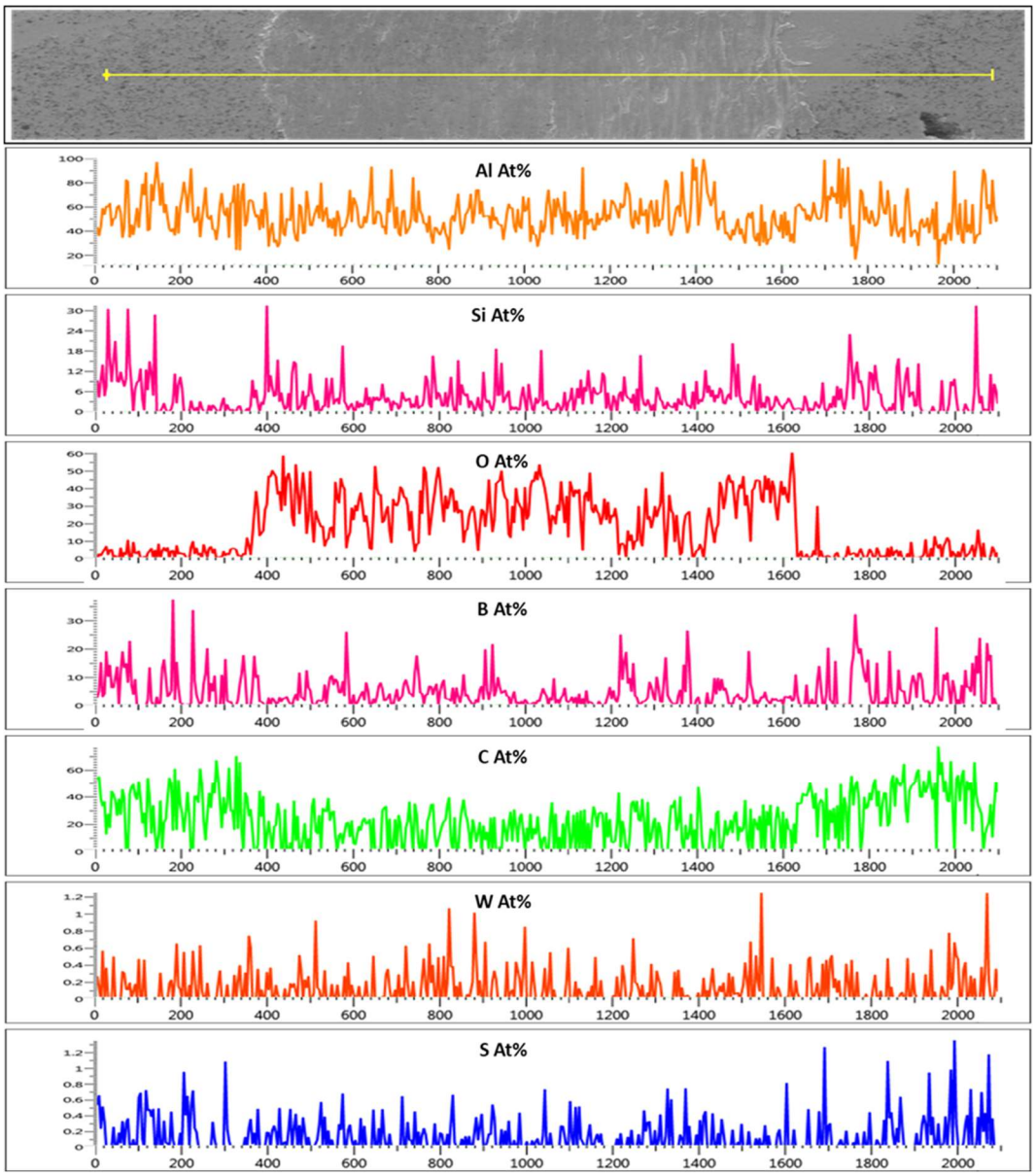


Figure 13. Graph of worn surfaces line EDS analysis of B319 + 10%B_4C + 0.5%WS_2 composite material.

Figure 14 displays the FE-SEM/MAP elemental mapping of the worn surface of the B319 + 10% B_4C + 2%WS_2 hybrid composite after the wear test. The mapping results demonstrate that the reinforcement particles (B_4C and WS_2) are uniformly distributed

across the wear track. The elements associated with the matrix (Al, Si) and reinforcements (B, C, W, S) are distinctly identified, and no significant clustering or segregation is observed.

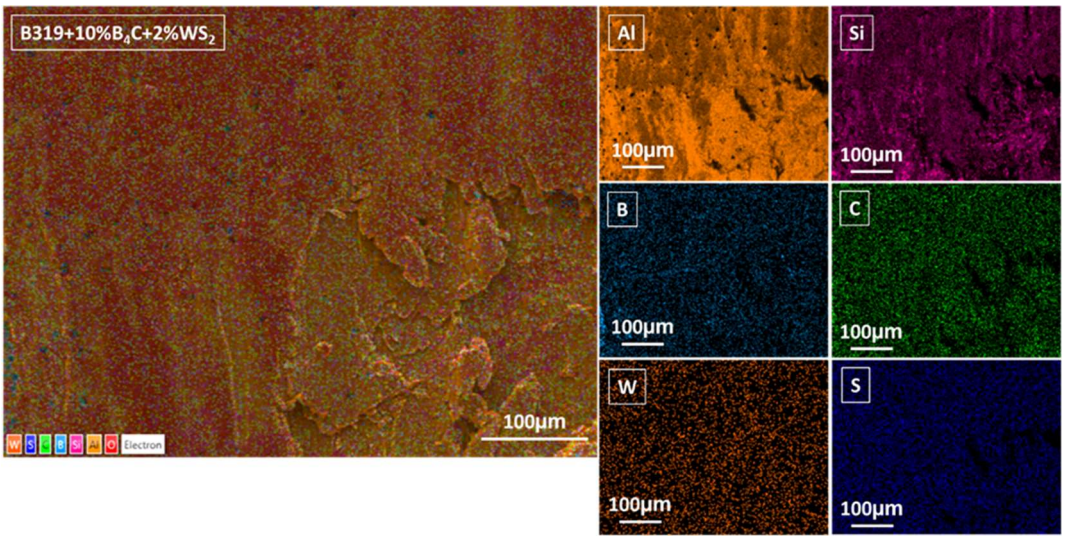


Figure 14. FE-SEM/MAP elemental analysis of the worn surface of B319 + 10%B_4C + 2%WS_2 hybrid composite.

Of particular importance is the evident distribution of WS_2-related elements (W and S), which supports the formation of a stable tribological film across the surface. The presence of B_4C, known for its high hardness, along grain boundaries, enhances resistance to abrasive wear, while the lubricating action of WS_2 contributes to a more ductile wear mechanism. These findings align with previous observations and further underline the synergistic effect of hybrid reinforcement on wear resistance [59].

The uniform elemental distribution revealed by MAP analysis further confirms the successful dispersion and retention of reinforcements during sliding. In particular, the simultaneous detection of B, C, W, and S across the worn surface suggests that both B_4C and WS_2 actively participate in the tribological response. B_4C acts as micro-scale wear-resistant barriers embedded within the matrix, while WS_2 continuously renews the lubricating tribo-film. The absence of localized clustering or elemental depletion zones indicates that the hybrid structure maintains its functional integrity even after significant sliding distances, contributing to both mechanical and tribological robustness.

Figure 15 presents the results of 3D optical profilometer analysis on the worn surfaces of unreinforced and reinforced B319 alloys. For the unreinforced B319 alloy, the average surface roughness (Ra) was measured at 0.124 µm. Despite appearing relatively smooth, this may be misleading, as it is thought that delaminated material re-adhered to the surface during sliding, thereby masking deeper surface damage. In the B319 + 10%B_4C composite, Ra increased sharply to 0.292 µm. This rise reflects the presence of more pronounced wear tracks and grooves caused by hard B_4C particles interacting abrasively with the counterface. The sharply varying height profiles also indicate a dominant abrasive wear mechanism.

Hybrid composites exhibited improved surface topography. In the B319 + 10%B_4C + 0.5%WS_2 sample, Ra decreased to 0.249 µm. Although some deep grooves were still present, particularly around embedded B_4C particles, the overall wear pattern was more stable. Notably, the B319 + 10%B_4C + 2%WS_2 sample achieved the lowest Ra value (0.159 µm), suggesting the smoothest wear surface. This improvement is associated with the solid lubricating action of WS_2, which reduces metal-to-metal contact and surface deterioration by forming a protective tribo-film. Moreover, the consistent difference between peak height and valley depth in this sample indicates uniform sliding behavior and reduced surface

roughness, correlating well with the low CoF and SWR observed. These results are in strong agreement with previous FE-SEM, MAP/EDS, and tribological findings, highlighting the effectiveness of hybrid reinforcement in enhancing both wear resistance and surface integrity [60].

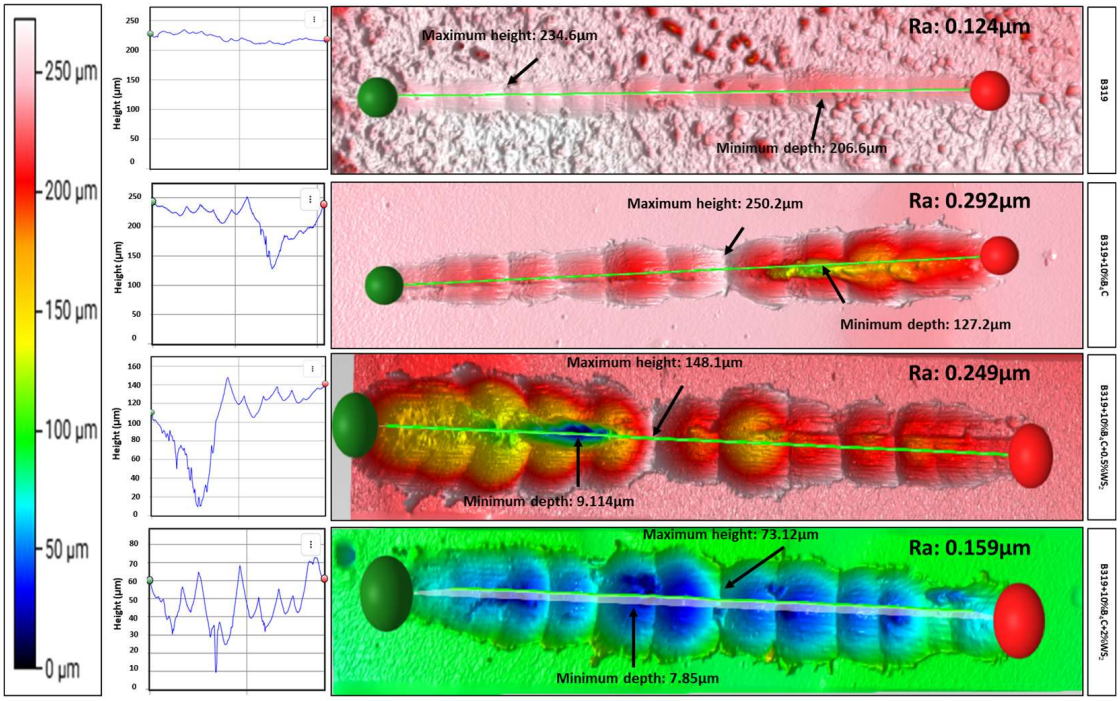


Figure 15. Three-dimensional & surface profilometry analysis of worn surfaces showing surface roughness (Ra) and wear morphology of B319 and hybrid/composite materials.

The profilometry data confirm that the addition of WS_2 significantly alters the surface damage mechanisms from deep abrasive grooving (in B_4C-only composites) to shallow, uniform wear tracks in hybrid composites. The lower Ra values observed in WS_2-reinforced samples are indicative of less severe material removal and smoother tribological contact, which correspond directly to the observed decreases in CoF and SWR. Furthermore, the minimization of surface roughness is critical for applications requiring tight tolerance control and reduced frictional losses, thereby broadening the potential applicability of these hybrid composites in advanced engineering systems. For the B319 alloy without reinforcement, the relatively smooth profilometry traces obtained despite the higher friction coefficient indicate the possibility of adhesive wear and possible delamination. The re-adhesion of the worn material particles to the surface during this process may have caused the surface roughness (Ra) to appear lower than it is. In contrast, the B319 + 10%B_4C composite exhibits a somewhat rough surface characterized by sharp peaks and deep valleys; this is thought to be a transition to a dominant abrasive wear mechanism as a result of the contact of the rigid ceramic reinforcement B_4C with the Al_2O_3 counter surface. The low Ra value and shallow, regular wear traces observed in the hybrid composites, especially in the sample containing 2% WS_2, reflect the transition to a wear regime mediated by tribo-film. In this structure, the solid lubricant layers of WS_2 reduce the contact of the directly contacting asperities and provide smoother sliding; This reduces wear volume and surface deterioration. When all the findings are evaluated, the wear mechanisms are predominantly abrasive in the B_4C-reinforced composites. At the same time, they evolve to more mixed mode or boundary lubrication behavior in the hybrid composites containing WS_2.

4. Conclusions

In this study, hybrid B319 aluminum matrix composites containing 10 wt% B_4C and different proportions of WS_2 (0.5 and 2 wt%) were synthesized via powder metallurgy followed by hot pressing. The resulting materials were subjected to detailed microstructural, mechanical, and tribological analyses, which yielded the following key findings:

SEM, XRD, and EDS analyses confirmed the spherical morphology and phase composition of B319 matrix powders, with Al, Si, and Al_2Cu phases identified. The hybrid reinforcement of B_4C and WS_2 was homogeneously distributed on the matrix surface without agglomeration, as verified by MAP and grain size analysis. The effective use of a 3D mixer facilitated uniform reinforcement dispersion, minimizing porosity and ensuring interfacial bonding.

FE-SEM and mapping analyses of sintered samples revealed that all reinforcements maintained structural integrity without forming voids or segregations. The B_4C particles effectively resisted grain boundary deformation, while WS_2 particles contributed to a smoother microstructure by reducing interfacial damage and enhancing load distribution.

The addition of reinforcements significantly improved hardness and transverse rupture strength (TRS). The microhardness increased from 80.5 HV in unreinforced B319 to 104.3 HV in the B319 + 10%B_4C + 2%WS_2 sample. Likewise, TRS rose from 163.8 MPa (B319) to 196.3 MPa (B319 + 10%B_4C + 2%WS_2), indicating the reinforcing effect of B_4C and the crack-arresting behavior of WS_2. These mechanical improvements are directly linked to the dual strengthening mechanisms introduced by the hybrid reinforcement: Orowan strengthening by B_4C particles and energy dissipation through WS_2-mediated crack path deflection.

The wear resistance of the composites improved markedly with reinforcement additions. The hybrid sample with 2 wt% WS_2 exhibited the lowest weight loss (0.0057 g) and specific wear rate (4.34×10^{-6} $mm^3/N{\cdot}m$), attributed to the solid lubricating nature of WS_2 and its role in forming a tribo-film on the wear surface. Friction coefficients declined from 0.497 μ in B319 to 0.178 μ in the 2% WS_2 hybrid composite, confirming the efficacy of WS_2 in reducing interfacial shear. The combination of hard B_4C phases for load-bearing and lubricating WS_2 phases for interfacial stabilization resulted in a significant shift from severe adhesive wear towards a mild abrasive and lubricated wear regime.

FE-SEM analysis of worn surfaces revealed a transition from adhesive and delamination wear in unreinforced B319 to abrasive and micro-ploughing wear in B_4C-reinforced samples. The introduction of WS_2 altered the wear mechanism towards a more ductile and lubricated regime with the presence of tribo-layers and reduced groove depth. EDS and mapping analyses supported the presence of WS_2 and B_4C within the wear track. Furthermore, 3D profilometry analyses confirmed that the incorporation of WS_2 significantly reduced surface roughness and wear-induced topographical irregularities, promoting more stable and homogeneous sliding behavior.

Although slight reductions in relative density were observed with increasing WS_2 content, these did not result in a measurable decline in microhardness, indicating that the level of densification attained was adequate to sustain the structural compactness and resistance to localized deformation. This supports the conclusion that incorporating WS_2 did not compromise the mechanical integrity in terms of hardness. While the thickness and chemical nature of the tribo-film could not be fully characterized due to equipment limitations, surface morphology, and EDS data provided supportive evidence for its formation. This study, therefore, not only validates the dual-functionality of B_4C and WS_2 in B319 matrix composites but also addresses a notable research gap by quantitatively demonstrating the mechanical and tribological enhancements offered by this specific hybrid reinforcement strategy, which has not been previously explored in B319 alloys. Integrating a challenging

ceramic phase (B_4C) and a solid lubricant (WS_2) presents a promising pathway for developing lightweight, high-performance aluminum matrix composites suitable for advanced automotive, aerospace, and marine applications.

Funding: This study has been financially supported by the Gazi University Scientific Research Projects Coordination Unit [under Project Number FGA-2025-9782].

Data Availability Statement: The original contributions presented in this study are included in the article. Further inquiries can be directed to the corresponding author.

Conflicts of Interest: The author declares no conflicts of interest.

References

1. Pillari, L.K.; Lessoway, K.; Bichler, L. Reciprocating Dry Sliding Friction and Wear Behavior of B319 Aluminum Alloy-Graphene Composites. *Tribol. Int.* **2024**, *192*, 109334. [CrossRef]
2. Wu, X.; Zhang, W. A Review on Aluminum Matrix Composites' Characteristics and Applications for Automotive Sector. *Heliyon* **2024**, *10*, e38576. [CrossRef] [PubMed]
3. Kumar, V.; Bichler, L. Effect of TiC Powder Addition on the Grain Refinement Response of B319 Aluminium Alloy. In *Light Metals 2014*; Grandfield, J., Ed.; Springer International Publishing: Cham, Switzerland, 2016; pp. 207–211, ISBN 978-3-319-48144-9.
4. Prasad, A.; Mok, J.; Lafortune, L.; Bichler, L. Grain Refinement of B319 Alloy Using Spark Plasma Sintered Al–Ti–C Grain Refiners. *Trans. Indian Inst. Met.* **2018**, *71*, 2759–2763. [CrossRef]
5. Pillari, L.K.; Lessoway, K.; van der Kuur, C.; Lombardi, A.; Byczynski, G.; Bichler, L. Effect of Graphene on the Microstructure, Thermal Conductivity, and Tribological Behavior of Cast B319 Al Alloy. *Wear* **2024**, *538–539*, 205201. [CrossRef]
6. Singhal, V.; Shelly, D.; Babbar, A.; Lee, S.-Y.; Park, S.-J. Review of Wear and Mechanical Characteristics of Al-Si Alloy Matrix Composites Reinforced with Natural Minerals. *Lubricants* **2024**, *12*, 350. [CrossRef]
7. Karpasand, F.; Abbasi, A.; Ardestani, M. Effect of Amount of TiB2 and B4C Particles on Tribological Behavior of Al7075/B4C/TiB2 Mono and Hybrid Surface Composites Produced by Friction Stir Processing. *Surf. Coatings Technol.* **2020**, *390*, 125680. [CrossRef]
8. Gorshenkov, M.V.; Kaloshkin, S.D.; Tcherdyntsev, V.V.; Danilov, V.D.; Gulbin, V.N. Fabrication and Microstructure of Al-Based Hybrid Composite Reinforced by B4C and Ultra-Dispersed Tungsten. *Defect Diffus. Forum* **2011**, *309–310*, 249–254. [CrossRef]
9. Singh, N.; Belokar, R.M. Tribological Behavior of Aluminum and Magnesium-Based Hybrid Metal Matrix Composites: A State-of-Art Review. *Mater. Today Proc.* **2021**, *44*, 460–466. [CrossRef]
10. Yuan, J.; Yao, Y.; Zhuang, M.; Du, Y.; Wang, L.; Yu, Z. Effects of Cu and WS2 Addition on Microstructural Evolution and Tribological Properties of Self-Lubricating Anti-Wear Coatings Prepared by Laser Cladding. *Tribol. Int.* **2021**, *157*, 106872. [CrossRef]
11. Niste, V.B.; Ratoi, M.; Tanaka, H.; Xu, F.; Zhu, Y.; Sugimura, J. Self-Lubricating Al-WS2 Composites for Efficient and Greener Tribological Parts. *Sci. Rep.* **2017**, *7*, 14665. [CrossRef]
12. Fogagnolo, J.B.; Velasco, F.; Robert, M.H.; Torralba, J.M. Effect of Mechanical Alloying on the Morphology, Microstructure and Properties of Aluminium Matrix Composite Powders. *Mater. Sci. Eng. A* **2003**, *342*, 131–143. [CrossRef]
13. Süzer, İ.; Özçakıcı, Y.E.; Tekinşen, A.S.; Bayrak, K.G.; Mertdinç-Ülküseven, S.; Balcı-Çağıran, Ö.; Öveçoğlu, M.L.; Ağaoğulları, D. High Entropy (HfTiZrVNb)B2 Ceramic Particulate Reinforced Al Matrix Composites: Synthesis, Mechanical, Microstructural and Thermal Characterization. *Ceram. Int.* **2024**, *50*, 26583–26595. [CrossRef]
14. Park, B.; Lee, D.; Jo, I.; Lee, S.B.; Lee, S.K.; Cho, S. Automated Quantification of Reinforcement Dispersion in B4C/Al Metal Matrix Composites. *Compos. Part B Eng.* **2020**, *181*, 107584. [CrossRef]
15. Singh, R.; Shadab, M.; Dash, A.; Rai, R.N. Characterization of Dry Sliding Wear Mechanisms of AA5083/B4C Metal Matrix Composite. *J. Braz. Soc. Mech. Sci. Eng.* **2019**, *41*, 98. [CrossRef]
16. Gajević, S.; Miladinović, S.; Güler, O.; Özkaya, S.; Stojanović, B. Optimization of Dry Sliding Wear in Hot-Pressed Al/B4C Metal Matrix Composites Using Taguchi Method and ANN. *Materials* **2024**, *17*, 4056. [CrossRef] [PubMed]
17. Abbas, A.; Huang, S.-J. ECAP Effects on Microstructure and Mechanical Behavior of Annealed WS2/AZ91 Metal Matrix Composite. *J. Alloys Compd.* **2020**, *835*, 155466. [CrossRef]
18. Xiao, J.-K.; Zhang, W.; Zhang, C. Microstructure Evolution and Tribological Performance of Cu-WS2 Self-Lubricating Composites. *Wear* **2018**, *412–413*, 109–119. [CrossRef]
19. Danish, M.; Gupta, M.K.; Rubaiee, S.; Ahmed, A.; Korkmaz, M.E. Influence of Hybrid Cryo-MQL Lubri-Cooling Strategy on the Machining and Tribological Characteristics of Inconel 718. *Tribol. Int.* **2021**, *163*, 107178. [CrossRef]
20. Tasci, U.; Yilmaz, T.A.; Bostan, B. Investigation of Microstructure, Wear and Transverse Rupture Strength of WE43/Nano B4C Composites Produced by Powder Metallurgy Method. *Tribol. Int.* **2023**, *180*, 108231. [CrossRef]

21. Ayerdi, J.J.; Aginagalde, A.; Llavori, I.; Bonse, J.; Spaltmann, D.; Zabala, A. Ball-on-Flat Linear Reciprocating Tests: Critical Assessment of Wear Volume Determination Methods and Suggested Improvements for ASTM D7755 Standard. *Wear* **2021**, *470–471*, 203620. [CrossRef]
22. Wang, H.; Gu, D. Nanometric TiC Reinforced AlSi10Mg Nanocomposites: Powder Preparation by High-Energy Ball Milling and Consolidation by Selective Laser Melting. *J. Compos. Mater.* **2014**, *49*, 1639–1651. [CrossRef]
23. Huang, L.J.; Geng, L.; Peng, H.-X. Microstructurally Inhomogeneous Composites: Is a Homogeneous Reinforcement Distribution Optimal? *Prog. Mater. Sci.* **2015**, *71*, 93–168. [CrossRef]
24. Aqida, S.N.; Ghazali, M.I.; Hashim, J. Effect of Porosity on Mechanical Properties of Metal Matrix Composite: An Overview. *J. Teknol. Sci. Eng.* **2004**, *40*, 17–32. [CrossRef]
25. Prasad, A.; Lafortune, L.; Mok, J.; Bichler, L. An Investigation on Spark Plasma Sintering of a Carbon Black Grain Refiner for the Aluminum Alloy B319. *Trans. Indian Inst. Met.* **2019**, *72*, 1399–1403. [CrossRef]
26. Moghadasi, K.; Mohd Isa, M.S.; Ariffin, M.A.; Mohd Jamil, M.Z.; Raja, S.; Wu, B.; Yamani, M.; Bin Muhamad, M.R.; Yusof, F.; Jamaludin, M.F.; et al. A Review on Biomedical Implant Materials and the Effect of Friction Stir Based Techniques on Their Mechanical and Tribological Properties. *J. Mater. Res. Technol.* **2022**, *17*, 1054–1121. [CrossRef]
27. Zhou, Q.; Wang, J.; Misra, A.; Huang, P.; Wang, F.; Xu, K. Dislocations Interaction Induced Structural Instability in Intermetallic Al2Cu. *npj Comput. Mater.* **2017**, *3*, 24. [CrossRef]
28. Montealegre-Melendez, I.; Arévalo, C.; Ariza, E.; Pérez-Soriano, E.M.; Rubio-Escudero, C.; Kitzmantel, M.; Neubauer, E. Analysis of the Microstructure and Mechanical Properties of Titanium-Based Composites Reinforced by Secondary Phases and B4C Particles Produced via Direct Hot Pressing. *Materials* **2017**, *10*, 1240. [CrossRef]
29. Ozturk, K.; Gecu, R.; Karaaslan, A. Microstructure, Wear and Corrosion Characteristics of Multiple-Reinforced (SiC–B4C–Al2O3) Al Matrix Composites Produced by Liquid Metal Infiltration. *Ceram. Int.* **2021**, *47*, 18274–18285. [CrossRef]
30. Samal, P.; Raj, H.; Meher, A.; Surekha, B.; Vundavilli, P.R.; Sharma, P. Synergistic Effect of B4C and Multi-Walled CNT on Enhancing the Tribological Performance of Aluminum A383 Hybrid Composites. *Lubricants* **2024**, *12*, 213. [CrossRef]
31. Behnamian, Y.; Serate, D.; Aghaie, E.; Zahiri, R.; Tolentino, Z.; Niazi, H.; Mostafaei, A. Tribological Behavior of ZK60 Magnesium Matrix Composite Reinforced by Hybrid MWCNTs/B4C Prepared by Stir Casting Method. *Tribol. Int.* **2022**, *165*, 107299. [CrossRef]
32. Moustafa, E.B.; Melaibari, A.; Alsoruji, G.; Khalil, A.M.; Mosleh, A.O. Tribological and Mechanical Characteristics of AA5083 Alloy Reinforced by Hybridising Heavy Ceramic Particles Ta2C & VC with Light GNP and Al2O3 Nanoparticles. *Ceram. Int.* **2022**, *48*, 4710–4721. [CrossRef]
33. Kumar, T.S.; Shalini, S.; Petrů, J.; Mishra, M.K.; Jeyaprakash, N.; Kalita, K. Machine Learning-Driven Analysis of Erosion Resistance in ZrSiO4/Al2O3 Reinforced A356 Hybrid Composites: Integration of CART Algorithm with Taguchi Optimization. *J. Mater. Res. Technol.* **2025**, *36*, 157–172. [CrossRef]
34. Freschi, M.; Di Virgilio, M.; Zanardi, G.; Mariani, M.; Lecis, N.; Dotelli, G. Employment of Micro-and Nano-WS2 Structures to Enhance the Tribological Properties of Copper Matrix Composites. *Lubricants* **2021**, *9*, 53. [CrossRef]
35. Vaziri, H.S.; Shokuhfar, A.; Afghahi, S.S.S. Synthesis of WS2/CNT Hybrid Nanoparticles for Fabrication of Hybrid Aluminum Matrix Nanocomposite. *Mater. Res. Express* **2020**, *7*, 25034. [CrossRef]
36. Wang, Y.; Liu, Q.; Zhang, B.; Zhang, H.; Zhong, Z.; Ye, J.; Ren, Y.; Shen, L.; Ye, F.; Wang, W. Mechanical Response and Damage Evolution of Bio-Inspired B4C-Reinforced 2024Al Composites Subjected to Quasi-Static and Dynamic Loadings. *Mater. Sci. Eng. A* **2022**, *840*, 142991. [CrossRef]
37. Ramesh, B.R.; Rajendran, C.; Saiyathibrahim, A.; Velu, R. Influence of B4C and ZrB2 Reinforcements on Microstructural, Mechanical and Wear Behaviour of AA 2014 Aluminium Matrix Hybrid Composites. *Def. Technol.* **2024**, *40*, 242–254. [CrossRef]
38. Çelebi, M.; Çanakçı, A.; Özkaya, S. Effect of Mechanical Milling Time on Powder Characteristic, Microstructure, and Mechanical Properties of AA2024/B4C/GNPs Hybrid Nanocomposites. *Powder Technol.* **2025**, *449*, 120439. [CrossRef]
39. Yu, Z.; Chen, M.; Kong, X.; Sun, W.; Wang, F. Achieving Well-Balanced Mechanical and Tribological Properties of Copper Matrix Self-Lubricating Composites by Adding Pre-Metallized B4C Particles with Core-Shell Microstructure. *Ceram. Int.* **2023**, *49*, 20613–20622. [CrossRef]
40. Tu, Y.; Zhang, L.; Zhang, X.; Kang, X. Improving the Mechanical and Tribological Behavior of Cu-WS2 Self-Lubricating Composite with the Addition of WS2 Nanosheet. *Wear* **2023**, *530*, 205013. [CrossRef]
41. Huang, S.-J.; Peng, W.-Y.; Visic, B.; Zak, A. Al Alloy Metal Matrix Composites Reinforced by WS2 Inorganic Nanomaterials. *Mater. Sci. Eng. A* **2018**, *709*, 290–300. [CrossRef]
42. Abebe Emiru, A.; Sinha, D.K.; Kumar, A.; Yadav, A. Fabrication and Characterization of Hybrid Aluminium (Al6061) Metal Matrix Composite Reinforced with SiC, B4C and MoS2 via Stir Casting. *Int. J. Met.* **2023**, *17*, 801–8012. [CrossRef]
43. Tan, J.L.; Liew, K.W. Tribological Behaviour and Microstructure of an Aluminium Alloy-Based g-SiC Hybrid Surface Composite Produced by FSP. *Lubricants* **2023**, *11*, 124. [CrossRef]

44. Gustavsson, F.; Jacobson, S. Diverse Mechanisms of Friction Induced Self-Organisation into a Low-Friction Material—An Overview of WS2 Tribofilm Formation. *Tribol. Int.* **2016**, *101*, 340–347. [CrossRef]
45. Liu, S.; Wang, Y.; Muthuramalingam, T.; Anbuchezhiyan, G. Effect of B4C and MOS2 Reinforcement on Micro Structure and Wear Properties of Aluminum Hybrid Composite for Automotive Applications. *Compos. Part B Eng.* **2019**, *176*, 107329. [CrossRef]
46. Li, P.; Aboulkhair, N.T.; Wu, J.; Leng, K.L.; Yang, D.; Clare, A.T.; Hou, X.; Xu, F. Tailoring the In-Situ Formation of Intermetallic Phases in the Self-Lubricating Al–WS2 Composite for Enhanced Tribological Performance with Wear Track Evolution Analysis. *J. Mater. Res. Technol.* **2023**, *27*, 4891–4907. [CrossRef]
47. Patil, N.A.; Pedapati, S.R.; Marode, R. V Wear Analysis of Friction Stir Processed AA7075-SiC-Graphite Hybrid Surface Composites. *Lubricants* **2022**, *10*, 267. [CrossRef]
48. Alizadeh, M.; Karimi, A.; Pashangeh, S.; Ostovari Moghaddam, A. Characterization of Wear and Corrosion Behavior of Al/Cu/MoS2/WC Hybrid Metal Matrix Composite Fabricated via Accumulative Roll Bonding Process. *J. Mater. Res. Technol.* **2025**, *35*, 4647–4659. [CrossRef]
49. Wu, J.; Li, Z.; Luo, Y.; Li, Y.; Gao, Z.; Zhao, Y.; Wu, C.; Liao, Y.; Jin, M. The Effects of Double Ceramic Particles (B4C-SiC) on the Performance, Microstructure, and Friction-Wear Mechanisms of Copper-Based PM. *Tribol. Int.* **2022**, *175*, 107865. [CrossRef]
50. Rajeshshyam, R.; Venkatraman, R.; Raghuraman, S.; Bhaumik, S. Wear Characteristics and Sustainability of WS2 Solid Lubricant Deposited Layer on Al 6061-T6 Substrate under the Dry Sliding Conditions. *Tribol. Mater. Surfaces Interfaces* **2023**, *17*, 260–270. [CrossRef]
51. Kara, G.I.; Sezek, S.; Aksakal, B.; Macit, C.K.; Horlu, M. Effect of Sintering Temperature, Additive Ratios, and Reinforcement of Boron and Boron Carbide Particle Sizes on the Mechanical and Tribological Properties of the Synthesized Cu-Cr Hybrid Composites. *Tribol. Int.* **2024**, *199*, 110011. [CrossRef]
52. Zhu, J.; Qi, J.; Guan, D.; Ma, L.; Dwyer-Joyce, R. Tribological Behaviour of Self-Lubricating Mg Matrix Composites Reinforced with Silicon Carbide and Tungsten Disulfide. *Tribol. Int.* **2020**, *146*, 106253. [CrossRef]
53. Mishigdorzhiyn, U.; Semenov, A.; Ulakhanov, N.; Milonov, A.; Dasheev, D.; Gulyashinov, P. Microstructure and Wear Resistance of Hot-Work Tool Steels after Electron Beam Surface Alloying with B4C and Al. *Lubricants* **2022**, *10*, 90. [CrossRef]
54. Subramani, M.; Huang, S.-J.; Borodianskiy, K. Effect of WS2 Nanotubes on the Mechanical and Wear Behaviors of AZ31 Stir Casted Magnesium Metal Matrix Composites. *J. Compos. Sci.* **2022**, *6*, 182. [CrossRef]
55. Fan, X.; Wang, J.; Zhang, T.; Bao, M.; Wang, B.; Liu, Z.; Feng, Y. Study on the Electrical Friction Wear Properties of Ag-G-La2O3-WS2 Composites. *J. Mater. Eng. Perform.* **2025**, 1–12. [CrossRef]
56. Li, P.; Xu, F.; Robertson, S.; Zhou, Z.; Hou, X.; Clare, A.T.; Aboulkhair, N.T. Metallurgical Reactions and Tribological Properties of Self-Lubricating Al-WS2 Composites: Laser Powder Bed Fusion Vs. Spark Plasma Sintering. *Mater. Des.* **2022**, *216*, 110543. [CrossRef]
57. Philip, J.T.; Singh, K.; Kailas, S.V. Ti6Al4V Interacting with Al2O3 under Ambient and Vacuum Conditions: Effect of Plastic Deformation and Tribo-Chemical Reactions on Wear Mechanisms. *Wear* **2024**, *550–551*, 205404. [CrossRef]
58. Zhu, X.; Zhang, S.; Zhang, L.; He, Y.; Zhang, X.; Kang, X. Frictional Behavior and Wear Mechanisms of Ag/MoS2/WS2 Composite under Reciprocating Microscale Sliding. *Tribol. Int.* **2023**, *185*, 108510. [CrossRef]
59. Taşcı, U.; Yılmaz, T.A.; Karakoç, H.; Karabulut, Ş. Enhancing Wear Resistance and Mechanical Behaviors of AA7020 Alloys Using Hybrid Fe_3O_4-GNP Reinforcement. *Lubricants* **2024**, *12*, 215. [CrossRef]
60. Kumar, V.; Gautam, G.; Ankit; Mohan, A.; Mohan, S. Correlating Surface Topography of Relaxed Layer of ZA/ZrB2in Situ Composites to Wear and Friction. *Surf. Topogr. Metrol. Prop.* **2023**, *11*, 25006. [CrossRef]

Disclaimer/Publisher's Note: The statements, opinions and data contained in all publications are solely those of the individual author(s) and contributor(s) and not of MDPI and/or the editor(s). MDPI and/or the editor(s) disclaim responsibility for any injury to people or property resulting from any ideas, methods, instructions or products referred to in the content.